N73-24066

NASA TECHNICAL NOTE

NASA TN D-7296

NASA TN D-7296

CASE FILE
COPY

LONGITUDINAL AERODYNAMIC PARAMETERS OF THE KESTREL AIRCRAFT (XV-6A) EXTRACTED FROM FLIGHT DATA

by William T. Suit and James L. Williams

Langley Research Center
Hampton, Va. 23665

NATIONAL AERONAUTICS AND SPACE ADMINISTRATION • WASHINGTON, D. C. • JUNE 1973

1. Report No.	2. Government Accession No.	3. Recipient's Catalog No.
NASA TN D-7296		

4. Title and Subtitle	5. Report Date
LONGITUDINAL AERODYNAMIC PARAMETERS OF THE KESTREL AIRCRAFT (XV-6A) EXTRACTED FROM FLIGHT DATA	June 1973
	6. Performing Organization Code
7. Author(s)	8. Performing Organization Report No.
William T. Suit and James L. Williams	L-8703
	10. Work Unit No.
9. Performing Organization Name and Address	501-26-05-02
NASA Langley Research Center Hampton, Va. 23665	11. Contract or Grant No.
	13. Type of Report and Period Covered
12. Sponsoring Agency Name and Address	Technical Note
National Aeronautics and Space Administration Washington, D.C. 20546	14. Sponsoring Agency Code

15. Supplementary Notes

16. Abstract

Flight-test data have been used to extract the longitudinal aerodynamic parameters of a vectored-thrust aircraft. The results show that deflecting the thrust past 15° has an effect on the pitching-moment derivatives and tends to reduce the static stability. The trend toward reduction in the longitudinal stability also has been noted by the pilots conducting the flight tests.

17. Key Words (Suggested by Author(s))	18. Distribution Statement
Parameter extraction Maximum likelihood Aerodynamic coefficients	Unclassified – Unlimited

19. Security Classif. (of this report)	20. Security Classif. (of this page)	21. No. of Pages	22. Price*
Unclassified	Unclassified	40	$3.00

*For sale by the National Technical Information Service, Springfield, Virginia 22151

LONGITUDINAL AERODYNAMIC PARAMETERS OF THE KESTREL AIRCRAFT (XV-6A) EXTRACTED FROM FLIGHT DATA

By William T. Suit and James L. Williams
Langley Research Center

SUMMARY

Flight-test data have been used to extract the longitudinal aerodynamic parameters of the Kestrel aircraft. The aircraft configurations included thrust-jet angles of 0^{o}, 15^{o}, and 30^{o}, and Mach numbers of 0.43, 0.62, and 0.82. The results show that deflecting the thrust past 15^{o} has an effect on the pitching-moment derivatives. Deflecting the thrust downward decreases the longitudinal static stability parameter $-C_{m_{\alpha}}$ and generally decreases the damping-in-pitch parameter $-\left(C_{m_q} + C_{m_{\dot{\alpha}}}\right)$ for trim normal-force coefficient $-C_{Z,o}$ values greater than 0.2. The trend toward reduction in the longitudinal stability parameter also has been noted by the pilots during flights of the Kestrel.

INTRODUCTION

Analytical and simulator studies of the flight and handling qualities of aircraft require that accurate estimates of the aerodynamic parameters be used if the results are to be valid. One of the more accurate methods of obtaining aerodynamic parameters is from data obtained during flight tests. To provide aerodynamics for analytical and simulator studies, and also to provide numerical values for comparison with wind-tunnel data and theoretical estimates, parameters have been extracted from flight data for many years. In the past, many of the attempts yielded unacceptable results. At present, improvements in instrumentation and, particularly, the development of large-capacity high-speed computers have enabled the engineer to take advantage of the advanced mathematical methods of parameter extraction. Results from recent studies made at the Langley Research Center with an advanced extraction method are reported in references 1 to 3.

The purpose of the present study is to present the longitudinal aerodynamic parameters of the Kestrel aircraft from flight data for several airspeeds and thrust vector angles. The technique and program used in extracting the parameters are those of reference 4.

SYMBOLS

Values are given in both SI and U.S. Customary Units. The measurements and calculations were made in U.S. Customary Units.

a	acceleration, m/sec^2 (ft/sec^2)
$\bar{c}$	wing mean geometric chord, m (ft)
F_j	engine gross thrust, N (lb)
F_X, F_Z	aerodynamic forces along aircraft X and Z axes, respectively, N (lb)
g	acceleration due to gravity, m/sec^2 (ft/sec^2)
h	altitude, m (ft)
I	moment of inertia, $kg\text{-}m^2$ ($slug\text{-}ft^2$)
l_t	distance from aircraft center of gravity to mean aerodynamic chord of horizontal tail, m (ft)
M_j	pitching moment due to reaction jets, N-m (ft-lb)
M_Y	moment about Y body axis, N-m (ft-lb)
N_f	engine fan speed, percent of maximum speed
p	rate of roll, radians/sec or deg/sec
q	rate of pitch, radians/sec or deg/sec
r	rate of yaw, radians/sec or deg/sec
S	wing area, m^2 (ft^2)
u	velocity along X body axis, m/sec (ft/sec)
V	aircraft total velocity, m/sec (ft/sec)

v velocity along Y body axis, m/sec (ft/sec)

W_a intake mass flow, kg/sec (lb/sec)

W_t aircraft weight, N (lb)

w velocity along Z body axis, m/sec (ft/sec)

X_i individual state in complete state vector X

α angle of attack, radians or deg

δ_e tail-plane deflection, positive for aircraft nosedown, radians or deg

θ pitch angle, radians or deg

θ_j jet nozzle angle, degrees

ρ air density, kg/m^3 (slugs/ft^3)

ϕ roll angle, radians

C_L lift coefficient

C_m pitching-moment coefficient, $\dfrac{M_Y}{\frac{1}{2}\rho V^2 S\bar{c}}$

C_T thrust coefficient, $\dfrac{F_j}{\frac{1}{2}\rho V^2 S}$

C_X axial-force coefficient, $\dfrac{F_X}{\frac{1}{2}\rho V^2 S}$

C_Z normal-force coefficient, $\dfrac{F_Z}{\frac{1}{2}\rho V^2 S}$

$C_{Z_\alpha} = \dfrac{\partial C_Z}{\partial \alpha}$ $\quad C_{m_{\delta_e}} = \dfrac{\partial C_m}{\partial \delta_e}$

$C_{m_\alpha} = \dfrac{\partial C_m}{\partial \alpha}$ $\quad C_{Z_q} = \dfrac{\partial C_Z}{\partial \frac{q\bar{c}}{2V}}$

$$C_{X_\alpha} = \frac{\partial C_X}{\partial \alpha} \qquad C_{Z_{\delta_e}} = \frac{\partial C_Z}{\partial \delta_e}$$

$$C_{m_q} = \frac{\partial C_m}{\partial \frac{q\bar{c}}{2V}} \qquad C_{m_{\dot{\alpha}}} = \frac{\partial C_m}{\partial \frac{\dot{\alpha}\bar{c}}{2V}}$$

$$C_{L_\alpha} = \frac{\partial C_L}{\partial \alpha}$$

Subscripts:

a	aileron
c	computed
e	tail plane
f	measured flight
o	indicates coefficient at trim conditions
r	rudder
t	indicates state at trim conditions
X,Y,Z	coordinate axes

A dot over a symbol signifies a derivative with respect to time.

The following symbols are used only in the figures and the variables require redefinition because of the limited symbols available on computer prepared plots.

ALPHA = $\alpha - \alpha_t$, radians

AXI	acceleration along X body axis, m/sec^2 (ft/sec^2)
AZI	acceleration along Z body axis, m/sec^2 (ft/sec^2)

DE = $\delta_e - \delta_{e,t}$, radians

G acceleration due to gravity, m/sec2 (ft/sec2)

Q rate of pitch, radians/sec

THETA pitch angle, radians

U velocity along X body axis, m/sec (ft/sec)

W velocity along Z body axis, m/sec (ft/sec)

EQUATIONS OF MOTION

The equations of motion used in this study are referred to a body-axis system and are as follows:

X-direction:

$$\dot{u} = rv - qw - g \sin\theta + \frac{g}{W_t} F_j \cos\theta_j - \frac{W_a}{W_t} V \cos\alpha + \frac{1}{2}\rho V^2 S \frac{g}{W_t}\left[C_{X,o} + C_{X_\alpha}(\alpha - \alpha_t)\right]$$

Z-direction:

$$\dot{w} = qu - pv + g \cos\theta \cos\phi - \frac{g}{W_t} F_j \sin\theta_j - \frac{W_a}{W_t} V \sin\alpha$$

$$+ \frac{1}{2}\rho V^2 S \frac{g}{W_t}\left[C_{Z,o} + C_{Z_\alpha}(\alpha - \alpha_t) + C_{Z_{\delta_e}}(\delta_e - \delta_{e,t})\right]$$

Pitching moment:

$$\dot{q} = \frac{I_Z - I_X}{I_Y} pr + \frac{I_{XZ}}{I_Y}(r^2 - p^2) + \frac{M_j}{I_Y} + \frac{1}{2}\rho \frac{V^2 S\bar{c}}{I_Y}\left[C_{m_\alpha}(\alpha - \alpha_t)\right.$$

$$\left. + C_{m_q} \frac{q\bar{c}}{2V} + C_{m_{\dot{\alpha}}} \frac{\dot{\alpha}\bar{c}}{2V} + C_{m_{\delta_e}}(\delta_e - \delta_{e,t})\right]$$

The thrust F_j and the intake mass flow W_a were considered to be constant for each individual run. The values of F_j and W_a were calculated for the different flight

conditions by using the manufacturer's performance curves for the type of engine used in the flight tests. The values of F_j and W_a used in the equations of motion are listed in table I.

TEST AIRCRAFT AND EQUIPMENT

The test aircraft used in this flight investigation was a Hawker-Siddeley Kestrel (XV-6A). The Kestrel is a single-place, prototype, vectored-thrust, V/STOL strike-reconnaissance aircraft. A three-view drawing of the aircraft is shown as figure 1.

A single Rolls Royce Pegasus Mark 5 engine powers the Kestrel. The Pegasus is an axial-flow vectored-thrust turbofan engine with an uninstalled sea-level static thrust rating of 69 000 newtons (15 500 lb). Thrust is vectored through two pairs of controllable engine exhaust nozzles and is equally distributed between the forward nozzles which exhaust cool air from the fan and the aft nozzles which exhaust turbine air. The nozzles are mechanically interconnected and can be rotated, at rates up to 90^o/sec, to any position from fully aft $(\theta_j = 0^o)$ to 5^o forward of vertically downward $(\theta_j = 95^o)$. Nozzle angle is controlled by a single lever located inboard on the throttle quadrant which is the only additional control required for thrust vectoring in the Kestrel.

Control moments during nonvectored flight are provided by conventional aerodynamic surfaces. The ailerons and tail plane are powered by tandem hydraulic systems; the rudder is unpowered. Lateral control forces are provided by a nonlinear spring unit and longitudinal forces by a q-feel unit supplemented with a feel spring. A bobweight in the control run increases longitudinal maneuvering forces by 8.9 N/g (2 lb/g), and 4.9 N/rad/sec^2 (1.1 lb/rad/sec^2) for pitch acceleration.

During vectored flight, reaction control moments are added to those produced by the normal aerodynamic surfaces. Reaction control shutter valves located at the nose, tail, and wing tips are mechanically connected to their adjacent aerodynamic control surface and receive high-pressure engine bleed air as a function of engine nozzle angle. Full reaction control is provided at engine nozzle angles greater than 20^o. No stability augmentation system (SAS) is provided.

The pitching moment due to the reaction jets is given by

$$M_j = \left[1 - 2.14(1 - N_f)\right]\left|\frac{\theta_j}{20}\right| M_j'$$

where

$$\left|\frac{\theta_j}{20}\right| = 1 \qquad \left(\theta_j \geq 20^o\right)$$

and where M_j' is taken from figure 2. The information for figure 2 was taken from a manufacturer's report at the time of problem setup. Modifications to the aircraft probably have resulted in a different reaction jet curve. Since the reaction jets are not particularly effective over the Mach number range of the test, any differences that exist were not considered to be significant. Additional aircraft and engine data are presented in table II.

FLIGHT TESTS

The aircraft was flown at nominal Mach numbers of 0.82, 0.62, and 0.43 with three nozzle deflections of 0^o, 15^o, and 30^o, and at a constant thrust for each data run. The center-of-gravity shift is negligible for the Kestrel aircraft as the fuel is burned. The altitude for the flights was about 4.6 km (15 000 ft). At each configuration and airspeed, several runs were made with different combinations of elevator steps and pulses. The conditions tested are shown in table I. Data pertinent to this study, which was recorded during the flight tests, included longitudinal acceleration, a_X; normal acceleration, a_Z; total airspeed, V; fan speed, N_f; pitch attitude, θ; roll attitude, ϕ; pitch rate, q; yaw rate, r; roll rate, p; angle of attack, α; angle of sideslip, β; altitude, h; control surface positions (aileron δ_a, elevator δ_e, rudder δ_r); and time t. The full-scale range of the recording instruments and their response frequency is given in table III. A filter was used to limit the response frequency of the instruments. Most of the instruments had acceptable performance at higher response frequencies. However, the test engineers felt the limiting frequencies were much higher than the response frequencies of the states to be measured and the limiting filters would cut out any high-frequency noise that might have been introduced.

DATA PREPARATION AND PARAMETER EXTRACTION

All data were stored on an onboard magnetic tape recorder using wide band FM recording techniques. To increase channel capacity, two channels were time shared by using pulse-amplitude modulation recording techniques. The data tapes were digitized and the data from the accelerometers were corrected for instrument location. The α and β readings were corrected for the effects of aircraft angular rates. The commutated data were interpolated so that the values could be determined at common time points for all data quantities. The linear velocities along the vehicle body axes were calculated from the measured airspeed, angle of attack, and angle of sideslip. All the data were put on one data tape at a rate of 20 points per second. The tapes were then ready for use in the derivative extraction program. Additional details on preparation of flight data for the extraction program and the use of the extraction program are given in reference 1.

The parameter-estimation procedure used in this study is an iterative procedure which maximizes the conditional likelihood function L (aerodynamic parameters, weights, initial conditions):

$$L = \frac{1}{(2\pi)^{1/2}|R|^{1/2}} \exp\left[-\frac{1}{2}\sum_{i=1}^{N}(X_{if} - X_{ic})^{T}R^{-1}(X_{if} - X_{ic})\right]$$

where R is the estimate of the error covariance matrix and X is the vector describing the state of the aircraft. Maximizing the likelihood function minimizes the difference between the measured and calculated aircraft motions $(X_{if} - X_{ic})$. (See ref. 4.) The states used in the likelihood function were u, w, q, a_Z, and a_X. After the convergence of the likelihood function, for a given flight data record, the current extracted aerodynamic derivatives were examined. The derivatives were accepted as well determined if (a) the computed time histories of the aircraft motion were close to the measured time histories, (b) the change in derivatives was small for successive iterations, and (c) the standard deviation of each derivative was less than about one-tenth of the extracted value of the derivative.

RESULTS AND DISCUSSION

Presentation of Data

Data for the flight conditions listed in table I were used to determine a set of aerodynamic derivatives for each of the flight conditions. The measured and computed time histories for each flight condition are shown in figures 3 to 5. The computed time histories shown are those attained after the differences between the measured and calculated trajectories become constant. The figures show that in all cases, the computed time histories were generally in close agreement with the flight records. Table IV gives the standard deviations of the computed states from the measured states. The standard deviations of the individual fits can be seen to be less than the 3 percent of full-scale uncertainty in the measured data (see table III) and in many cases, the standard deviations were less than 1 percent of full scale of the measured quantity.

The derivatives extracted for each flight condition (the derivatives which resulted in the computed time histories of figs. 3 to 5) are listed in table V along with their standard deviations. It should be noted that the control parameter $C_{Z_{\delta_e}}$ was not extracted by the computer program. It was calculated from the extracted values of $C_{m_{\delta_e}}$ and use of the geometric relationship

$$C_{m_{\delta_e}} = \frac{l_t}{\bar{c}} C_{Z_{\delta_e}}$$

In addition, the extraction program indicated a very high correlation between C_{m_q} and $C_{m_{\dot{\alpha}}}$ so that table V shows the sum of the two parameters rather than numerical values for each.

Discussion of Results

The aerodynamic parameters of table V are plotted against trim normal-force coefficient in figure 6 for the Kestrel with each of the nozzle deflections. The data indicate that for each θ_j, the aerodynamic parameters vary linearly with normal-force coefficient. The normal-force coefficient contains both angle of attack and Mach number effects. Although the aerodynamic parameters appear to have a linear variation with normal-force coefficient for the flight data examined in this investigation, in general, some nonlinearity due to Mach number could be expected at the highest Mach number.

It should be noted that the thrust coefficient also varies with trim normal-force coefficient (table V) so that part of the change in parameters shown in figure 6 might be associated with thrust-coefficient variation. This possibility was examined by the use of wind-tunnel data from figure 7 of reference 5 (for zero nozzle deflection). These data were used to generate the curve shown in figure 7, which indicates the variation of C_{L_α} with thrust coefficient. The results indicate that C_{L_α} increases linearly with thrust coefficient. However, for the range of thrust coefficients of the present study (from 0.121 to 0.196), the expected change in C_{Z_α} should be small. The data of reference 5 did not show a clear-cut effect of thrust coefficient on C_{m_α}.

The static longitudinal stability parameter C_{m_α} (fig. 6) appears to increase (become more negative) as $C_{Z,o}$ increases. In addition, there is a large effect of nozzle deflection on this parameter. Increasing the nozzle deflection past 15^o caused a reduction in C_{m_α}. These effects were also noted in the $C_T = 0.2$ data of reference 5 and were substantiated by pilot opinion. Increasing the nozzle deflection also caused a decrease in the effective damping-in-pitch parameter $-\left(C_{m_q} + C_{m_{\dot{\alpha}}}\right)$ for values of $C_{Z,o}$ greater than -0.2 and nozzle deflections greater than 15^o.

There is very little published data with which to compare the results of this study. Reference 5 was concerned primarily with the low-speed high-nozzle-deflection configuration, but does have a limited amount of data for the configuration with zero nozzle deflection. The trim normal-force coefficients from the data of reference 5 are compared with those obtained in the present study in figure 8. The figure shows that the results of this study appear to be consistent as the thrust deflection varies and this study shows good agreement with the results of reference 5.

At a Mach number of 0.4, the data from reference 5 also indicate that the $C_{m_{\delta_e}}$ trends seem to be reasonable, although the magnitudes of $C_{m_{\delta_e}}$ obtained from reference 5 were more negative. The coefficient $C_{m_{\delta_e}}$ was also estimated by using an

approximate equation from reference 6 $\left(C_{Z_{\delta_e}} = \frac{W_t}{\bar{q}S}\frac{\Delta a_Z}{\Delta \delta_e}\right)$ and $C_{m_{\delta_e}}$ was then calculated by using $C_{m_{\delta_e}} = \frac{l_t}{\bar{c}} C_{Z_{\delta_e}}$. The same trends were observed and these results are shown in figure 9.

CONCLUDING REMARKS

Flight-test data have been used to extract the longitudinal aerodynamic parameters of the Kestrel aircraft. The aircraft configurations included thrust-jet angles of 0^o, 15^o, and 30^o, and Mach numbers of 0.43, 0.62, and 0.82. The results show that deflecting the thrust past 15^o has an effect on the pitching-moment derivatives. Deflecting the thrust downward decreases the longitudinal static stability parameter $-C_{m_\alpha}$ and generally decreases the damping-in-pitch parameter $-\left(C_{m_q} + C_{m_{\dot{\alpha}}}\right)$ for trim normal-force coefficient $-C_{Z,o}$ values greater than 0.2. The trend toward reduction in the longitudinal stability parameter also has been noted by the pilots during flights of the Kestrel.

Langley Research Center,
National Aeronautics and Space Administration,
Hampton, Va., May 7, 1973.

REFERENCES

1. Suit, William T.: Aerodynamic Parameters of the Navion Airplane Extracted From Flight Data. NASA TN D-6643, 1972.

2. Steinmetz, George G.; Parrish, Russell V.; and Bowles, Roland L.: Longitudinal Stability and Control Derivatives of a Jet Fighter Extracted From Flight Test Data by Utilizing Maximum Likelihood Estimation. NASA TN D-6532, 1972.

3. Williams, James L.: Extraction of Longitudinal Aerodynamic Coefficients From Forward-Flight Conditions of a Tilt-Wing V/STOL Airplane. NASA TN D-7114, 1972.

4. Grove, Randall D.; Bowles, Roland L.; and Mayhew, Stanley C.: A Procedure for Estimating Stability and Control Parameters From Flight Test Data by Using Maximum Likelihood Methods Employing a Real-Time Digital System. NASA TN D-6735, 1972.

5. Margason, Richard J.; Vogler, Raymond D.; and Winston, Matthew M.: Wind-Tunnel Investigation at Low Speeds of a Model of the Kestrel (XV-6A) Vectored-Thrust V/STOL Airplane. NASA TN D-6826, 1972.

6. Wolowicz, Chester H.: Considerations in the Determination of Stability and Control Derivatives and Dynamic Characteristics From Flight Data. AGARD Report 549 – Pt. I, 1966.

TABLE I.- TEST FLIGHT CONDITIONS

Nozzle angle, deg	Mach number	N_f, percent	F_j		W_a	
			N	lbf	N/sec	lbf/sec
0	0.82	0.85	55 300	12 400	1300	287
0	.62	.75	33 000	7 400	1000	226
0	.43	.65	20 000	4 500	800	180
15	.82	.86	57 000	13 000	1286	289
15	.62	.76	34 000	7 700	1014	228
30	.82	.91	63 000	14 000	1334	300
30	.62	.82	40 000	8 900	1090	245
30	.43	.71	25 000	5 600	890	200

TABLE II.- GENERAL AIRCRAFT AND ENGINE DATA

Weights and inertia:	
Empty weight, N (lb)	45 390 (10 200)
Design gross weight, N (lb)	78 320 (17 600)
Maximum hovering weight, N (lb)	57 850 (13 000)
Total internal fuel, N (lb)	22 250 (5 000)
I_{ZZ} at 61 351.22 N (13 790 lbf), kg-m^2 (slug-ft^2)	3.322×10^4 (2.45×10^4)
I_{YY} at 61 351.22 N (13 790 lbf), kg-m^2 (slug-ft^2)	3.055×10^4 (2.25×10^4)
I_{XX} at 61 351.22 N (13 790 lbf), kg-m^2 (slug-ft^2)	0.545×10^4 (0.40×10^4)
I_{XZ} at 61 351.22 N (13 790 lbf), kg-m^2 (slug-ft^2)	0.231×10^4 (0.17×10^4)
Fuselage:	
Length, m (ft)	12.97 (42.54)
Height to top of vertical tail, m (ft)	3.28 (10.75)
Wetted area, net, m^2 (ft^2)	45.99 (495.0)
Wing:	
Area, gross, m^2 (ft^2)	17.32 (186.4)
Area, net, m^2 (ft^2)	12.27 (132.1)
Span, m (ft)	6.98 (22.9)
Mean aerodynamic chord, m (in.)	2.49 (98.0)
Dihedral angle, deg	-12.0
Taper ratio	0.40
Aspect ratio	2.8
Sweepback of leading edge, deg	40.0
Aileron area, m^2 (ft^2)	0.98 (10.54)
Left aileron travel limits:	
Trailing edge full down, deg	12.0
Trailing edge full up, deg	13.0
Trim range, deg	±3.5
Flap area (left and right), m^2 (ft^2)	1.23 (13.25)
Flap travel limit, deg	50
Tail plane:	
Area, gross, m^2 (ft^2)	4.41 (47.5)
Area, net, m^2 (ft^2)	3.84 (41.3)
Span, m (ft)	4.24 (13.92)
Aspect ratio	3.26
Dihedral angle, deg	-15.5
Standard mean chord, m (ft)	1.04 (3.41)
Tail plane travel limits:	
Trailing edge full down, deg	11.5
Trailing edge full up, deg	10.0
Trim range, deg	7.5 to -3.5

TABLE II.- GENERAL AIRCRAFT AND ENGINE DATA – Concluded

Vertical tail:
- Area, gross, m^2 (ft^2) 2.42 (26.1)
- Aspect ratio 1.22
- Rudder area, m^2 (ft^2) 0.509 (5.48)
- Rudder travel limits:
  - Trailing edge left and right, deg 15.0
  - Trim tab movement, deg . . . . . ±5.0

Reaction control system:
- Full noseup reaction pitch control at tail plane angle, deg 4.5
- Full pitch control, tail plane, deg 10.0
- Full roll control, aileron (total), deg . . . . . ±14
- Full yaw control, rudder, deg . . . . . ±10
- Pitch reaction control arm about c.g.:
  - Pitch noseup, m (ft) 4.62 (15.15)
  - Pitch nosedown, m (ft) 7.26 (23.83)
- Roll reaction arm about center line, m (ft) 3.39 (11.12)
- Yaw reaction arm about c.g., m (ft) 7.08 (23.24)

Engine data:
- Number and model . . . . . Rolls Royce Pegasus Mark 5
- Type . . . . . Ducted-fan lift-thrust engine
- Intake area, m^2 (ft^2) 0.87 (9.3)
- Bypass ratio 1.4
- Maximum thrust, uninstalled sea level, N (lb) 69 000 (15 500)

Operating limitations:

Power rating	Reaction control bleed	N_f, percent	Exhaust gas temperature, ^oC	Time limit
Maximum	With bleed	93.5	645	2.5 min
	No bleed	93.5	595	2.5 min
Maximum continuous	With bleed	85.0	540	Unlimited
	No bleed	89.0	540	Unlimited

TABLE III.- RANGES AND RESPONSE FREQUENCY OF INSTRUMENTS

State	Range	Instrument response frequency, Hz
a_X	±2g	6
a_Z	-2 to 8g	6
V	0 to 366 m/sec (0 to 1200 ft/sec)	2
θ	$\pm 60^o$	4
ϕ	$\pm 120^o$	4
q	$\pm 45^o$	6
r	$\pm 45^o$	6
p	$\pm 60^o$	6
α	-10^o to 30^o	4
β	$\pm 20^o$	4
h	0 to 182.9 km (0 to 60 000 ft)	2
δ_e	$\pm 11^o$	4

TABLE IV.- STANDARD DEVIATIONS OF THE CALCULATED RELATIVE STATES FROM THE MEASURED STATES AT CONVERGENCE

State	Standard deviations for nozzle angles of –								
	0°			15°			30°		
	M = 0.82	M = 0.62	M = 0.43	M = 0.82	M = 0.62	M = 0.43	M = 0.82	M = 0.62	M = 0.43
u	1.23 m/sec (4.02 ft/sec)	1.89 m/sec (6.20 ft/sec)	0.78 m/sec (2.55 ft/sec)	1.64 m/sec (5.37 ft/sec)	1.33 m/sec (4.37 ft/sec)	No data available	1.38 m/sec (4.53 ft/sec)	0.94 m/sec (3.10 ft/sec)	0.84 m/sec (2.76 ft/sec)
w	1.37 m/sec (4.51 ft/sec)	1.24 m/sec (4.06 ft/sec)	0.76 m/sec (2.50 ft/sec)	1.27 m/sec (4.17 ft/sec)	1.23 m/sec (4.04 ft/sec)	↓	1.20 m/sec (3.95 ft/sec)	1.61 m/sec (5.29 ft/sec)	2.01 m/sec (6.60 ft/sec)
q	0.57 deg/sec	0.73 deg/sec	0.41 deg/sec	0.67 deg/sec	0.61 deg/sec	↓	0.75 deg/sec	0.775 deg/sec	1.12 deg/sec
a_X	0.19 m/sec^2 (0.63 ft/sec^2)	0.34 m/sec^2 (1.12 ft/sec^2)	0.09 m/sec^2 (0.30 ft/sec^2)	0.12 m/sec^2 (0.40 ft/sec^2)	0.25 m/sec^2 (0.83 ft/sec^2)	↓	0.24 m/sec^2 (0.79 ft/sec^2)	0.32 m/sec^2 (1.05 ft/sec^2)	0.22 m/sec^2 (0.72 ft/sec^2)
a_Z	1.97 m/sec^2 (6.46 ft/sec^2)	1.28 m/sec^2 (4.19 ft/sec^2)	0.40 m/sec^2 (1.30 ft/sec^2)	1.27 m/sec^2 (4.16 ft/sec^2)	0.74 m/sec^2 (2.42 ft/sec^2)	↓	1.15 m/sec^2 (3.76 ft/sec^2)	1.29 m/sec^2 (4.22 ft/sec^2)	1.03 m/sec^2 (3.39 ft/sec^2)

TABLE V.- EXTRACTED AERODYNAMIC PARAMETERS AND STANDARD DEVIATION

[Standard deviations are given in parentheses]

Parameter	Extracted aerodynamic parameters and standard deviation for –							
	$\theta_j = 0^o$ $M \approx 0.82$ $C_T = 0.121$ $\alpha = 1.75^o$	$\theta_j = 0^o$ $M \approx 0.62$ $C_T = 0.121$ $\alpha = 3.33^o$	$\theta_j = 0^o$ $M \approx 0.43$ $C_T = 0.155$ $\alpha = 8.94^o$	$\theta_j = 15^o$ $M \approx 0.82$ $C_T = 0.1195$ $\alpha = 0.722^o$	$\theta_j = 15^o$ $M \approx 0.62$ $C_T = 0.128$ $\alpha = 4.70^o$	$\theta_j = 30^o$ $M \approx 0.82$ $C_T = 0.139$ $\alpha = 0.653^o$	$\theta_j = 30^o$ $M \approx 0.62$ $C_T = 0.151$ $\alpha = 2.22^o$	$\theta_j = 30^o$ $M \approx 0.43$ $C_T = 0.196$ $\alpha = 7.91^o$
$C_{Z,o}$	-0.13 ± 0.0012	-0.225 ± 0.002	-0.46 ± 0.0014	-0.068 ± 0.0013	-0.21 ± 0.0014	-0.042 ± 0.0012	-0.127 ± 0.0021	-0.37 ± 0.0031
C_{Z_α}	-2.82 ± 0.07	-3.04 ± 0.105	-2.83 ± 0.03	-2.92 ± 0.064	-2.26 ± 0.064	-2.95 ± 0.041	-2.67 ± 0.067	-2.58 ± 0.058
$C_{Z_{\delta_e}}$	-0.42	-0.50	-0.63	-0.405	-0.47	-0.42	-0.33	-0.12
$C_{X,o}$	-0.029 ± 0.0002	-0.01 ± 0.0004	0.034 ± 0.0003	-0.03 ± 0.0001	-0.015 ± 0.0002	-0.027 ± 0.0002	-0.015 ± 0.0004	0.02 ± 0.0006
C_{X_α}	0.23 ± 0.0067	0.32 ± 0.013	0.535 ± 0.0056	0.23 ± 0.0049	0.26 ± 0.0078	0.186 ± 0.0052	0.29 ± 0.0084	0.43 ± 0.0095
C_{m_α}	-0.13 ± 0.0035	-0.167 ± 0.0046	-0.28 ± 0.0035	-0.14 ± 0.0034	-0.137 ± 0.0016	-0.059 ± 0.0008	-0 055 ± 0.0011	-0.097 ± 0.0014
$C_{m_q} + C_{m_{\dot\alpha}}$	-10.44 ± 0.70	-10.79 ± 0.75	-14.90 ± 0.39	-11.61 ± 0.68	-11.82 ± 0.42	-12.82 ± 0.46	-9.75 ± 0.45	-5.15 ± 0.32
$C_{m_{\delta_e}}$	-0.91 ± 0.034	-1.07 ± 0.04	-1.37 ± 0.022	-0.87 ± 0.036	-1.02 ± 0.027	-0.901 ± 0.027	-0.707 ± 0.027	-0.257 ± 0.016

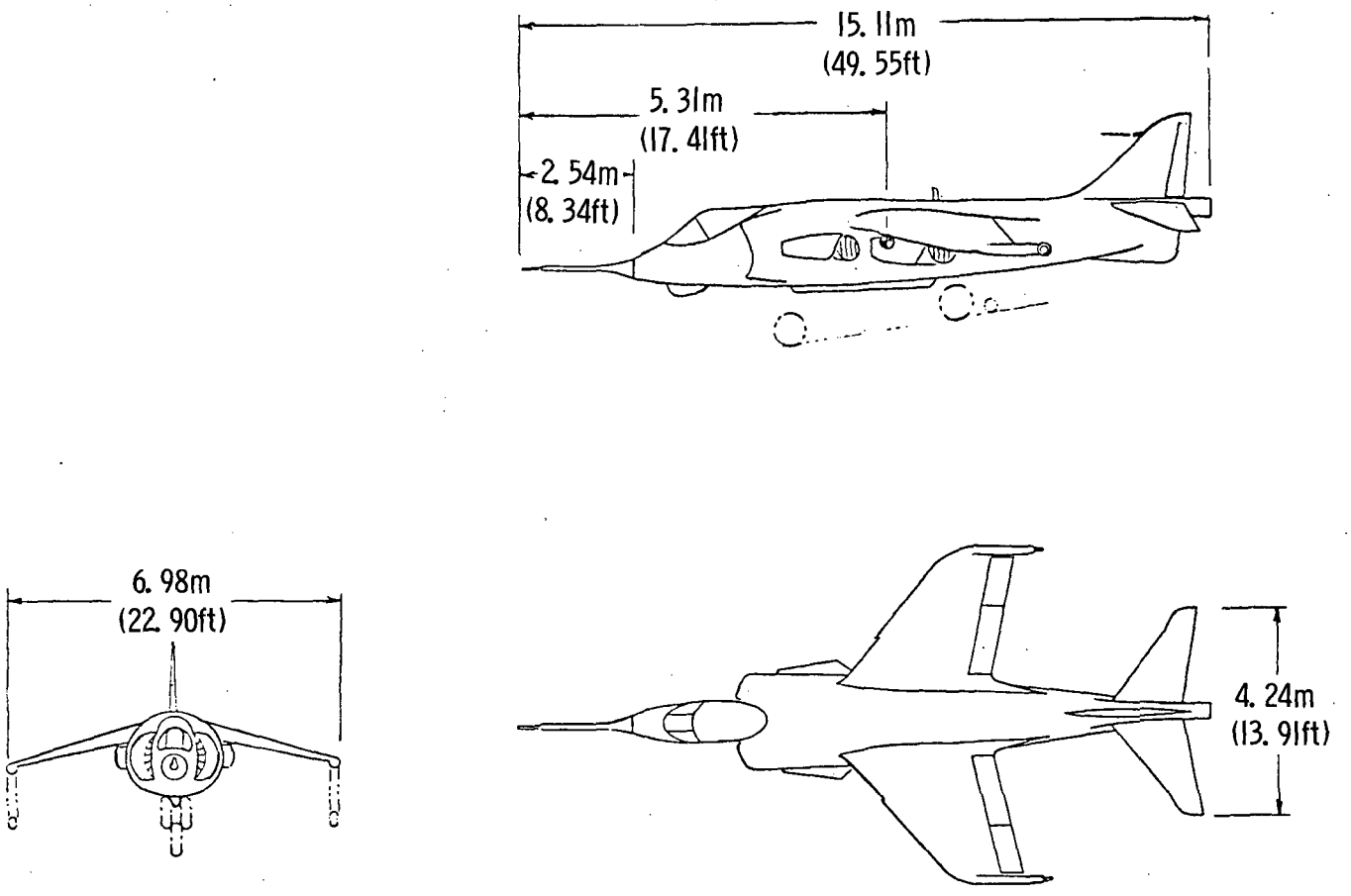

Figure 1.- Three-view drawing of test airplane.

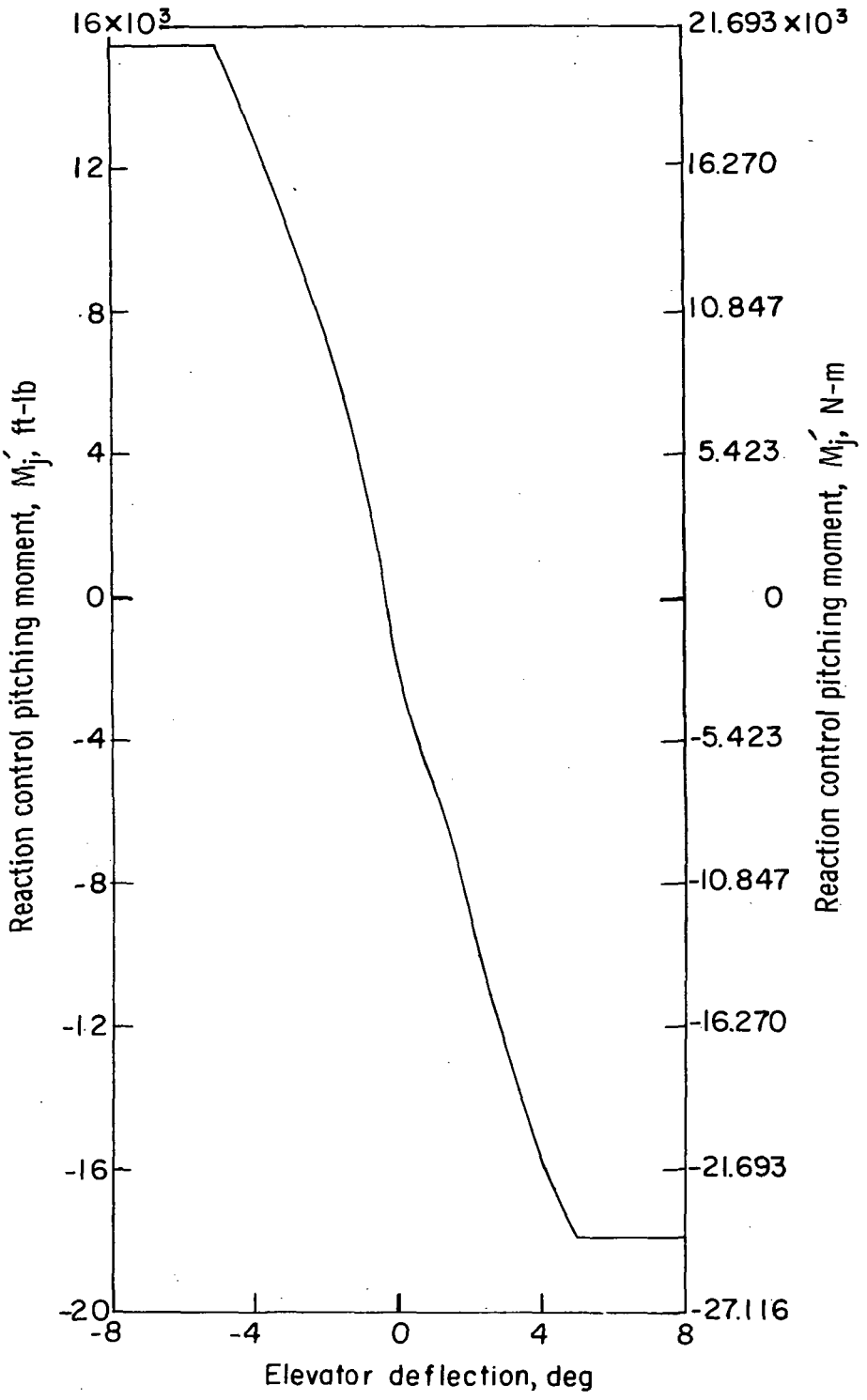

Figure 2.- Variation in reaction control pitching moment with elevator deflection.

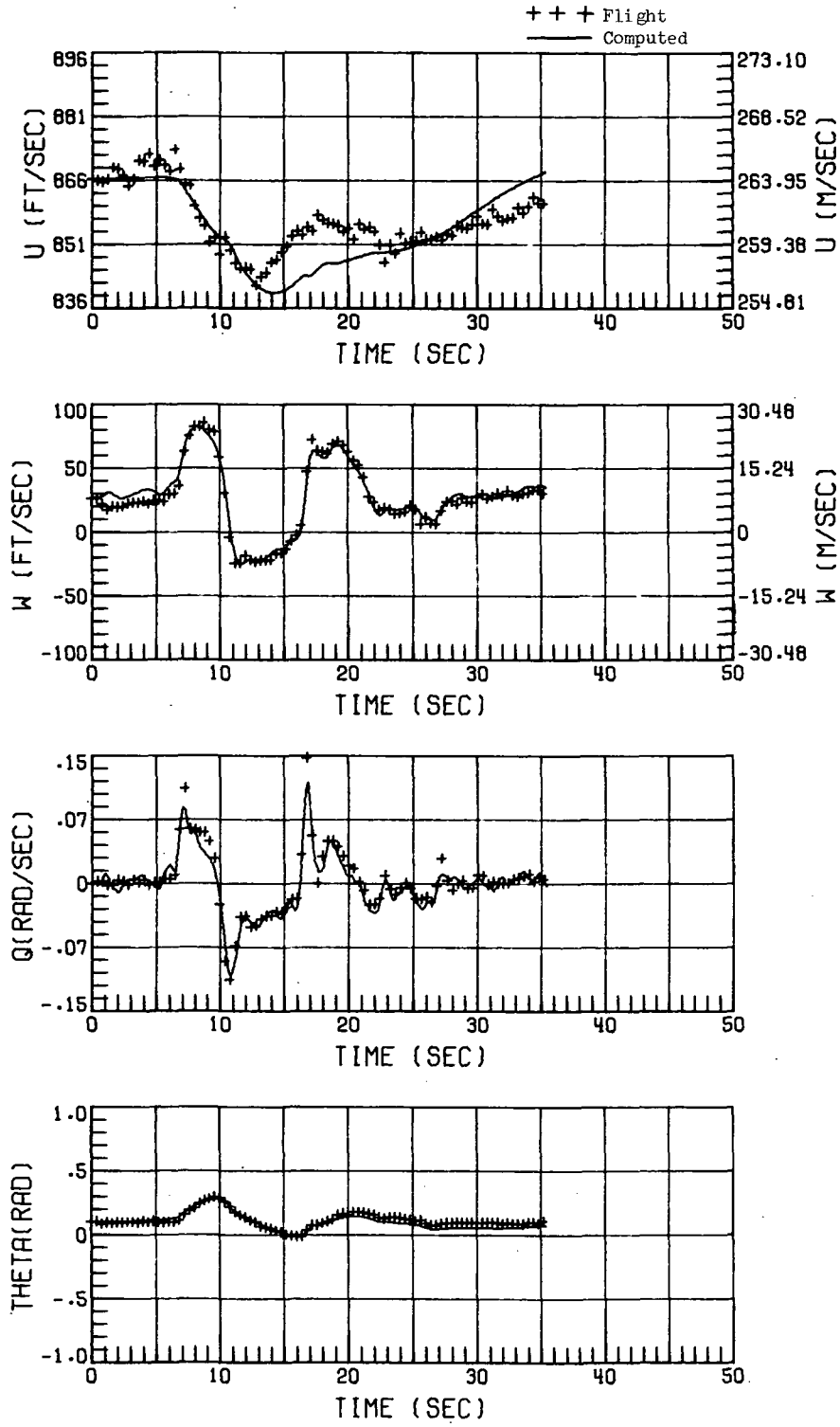

(a) $\theta_j = 0^o$.

Figure 3.- Comparison of flight data with time histories computed by using the aerodynamic parameters of table V for an elevator input. Mach number, 0.82.

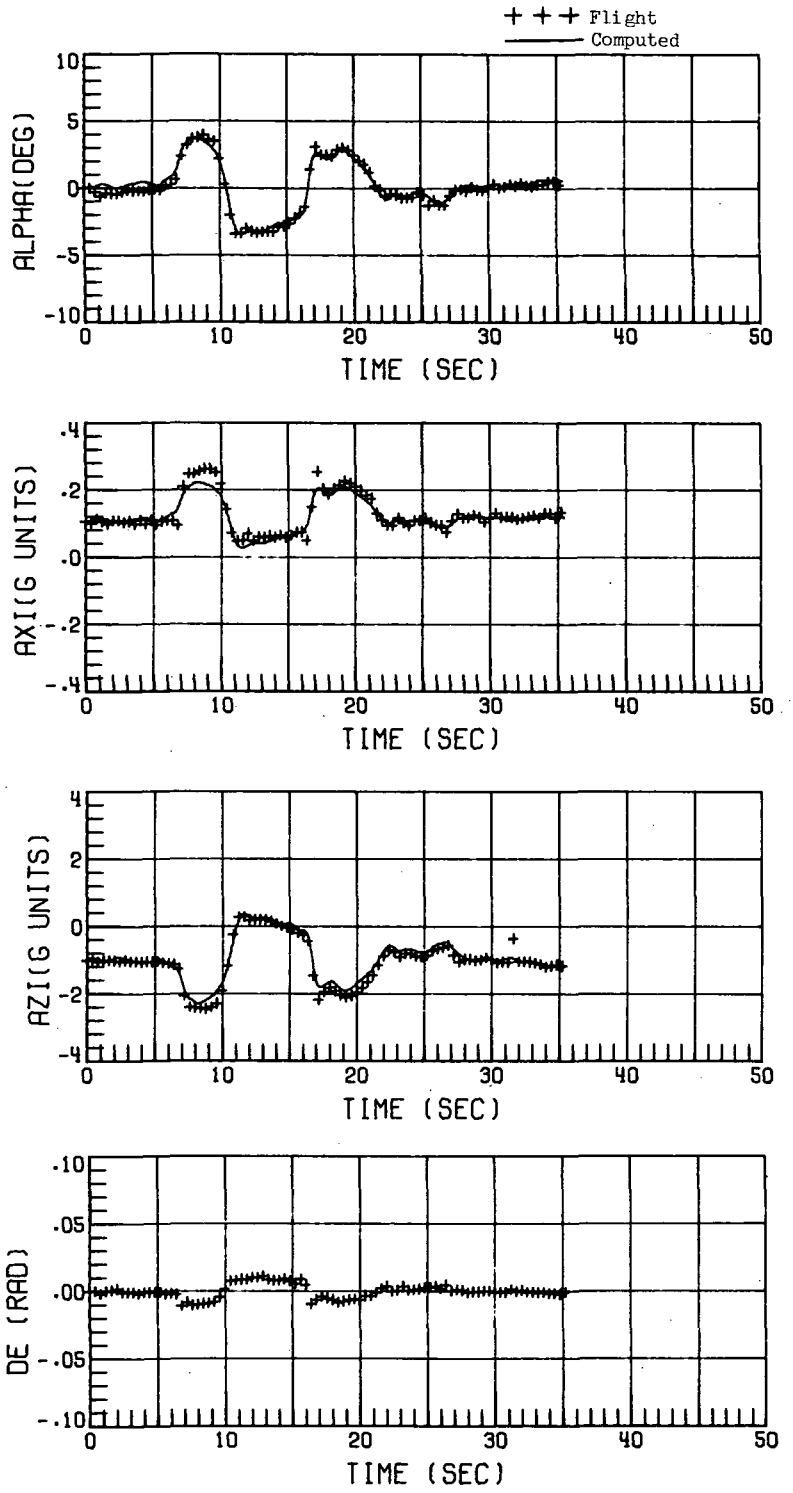

(a) $\theta_j = 0^o$. Concluded.

Figure 3.- Continued.

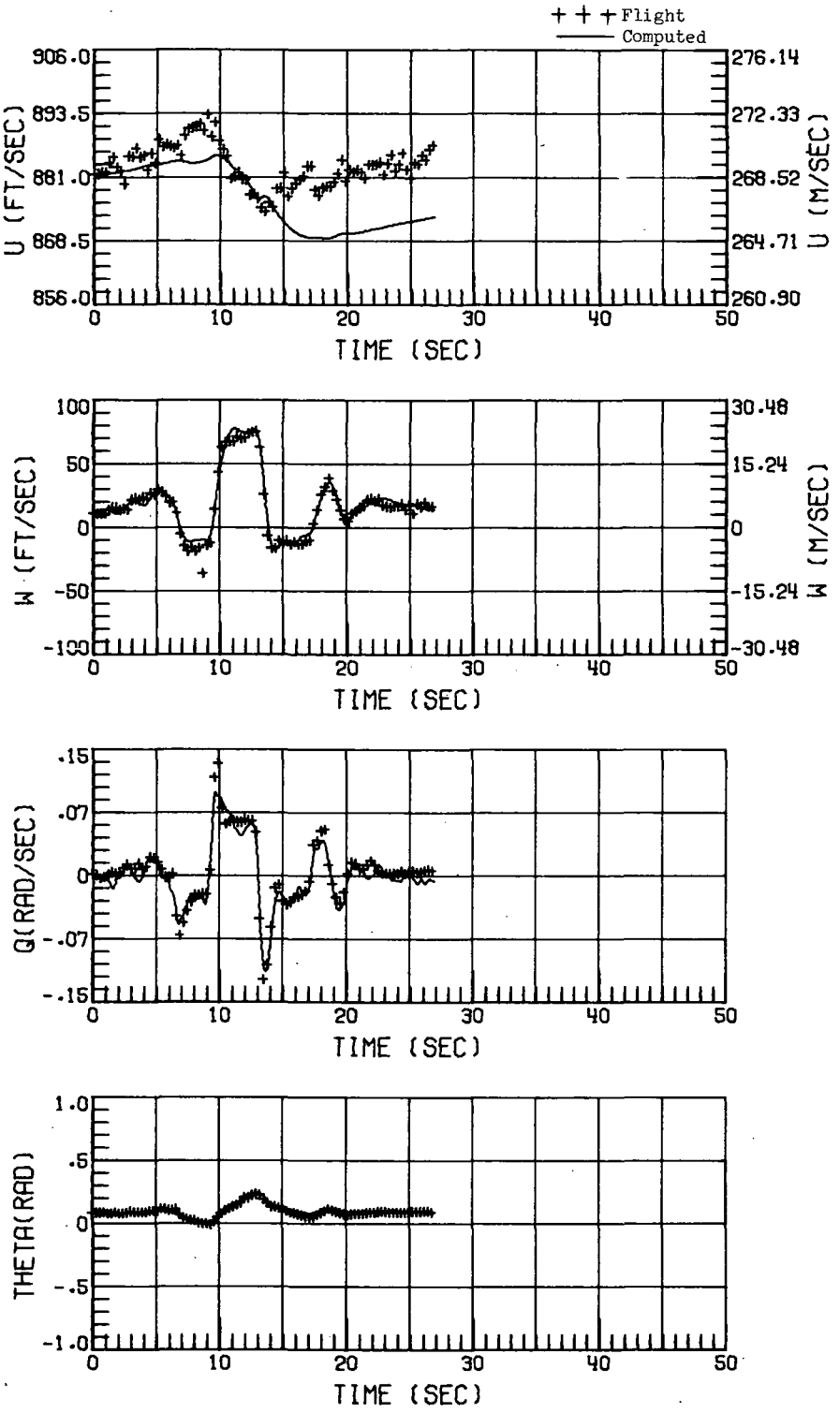

(b) $\theta_j = 15^o$.

Figure 3.- Continued.

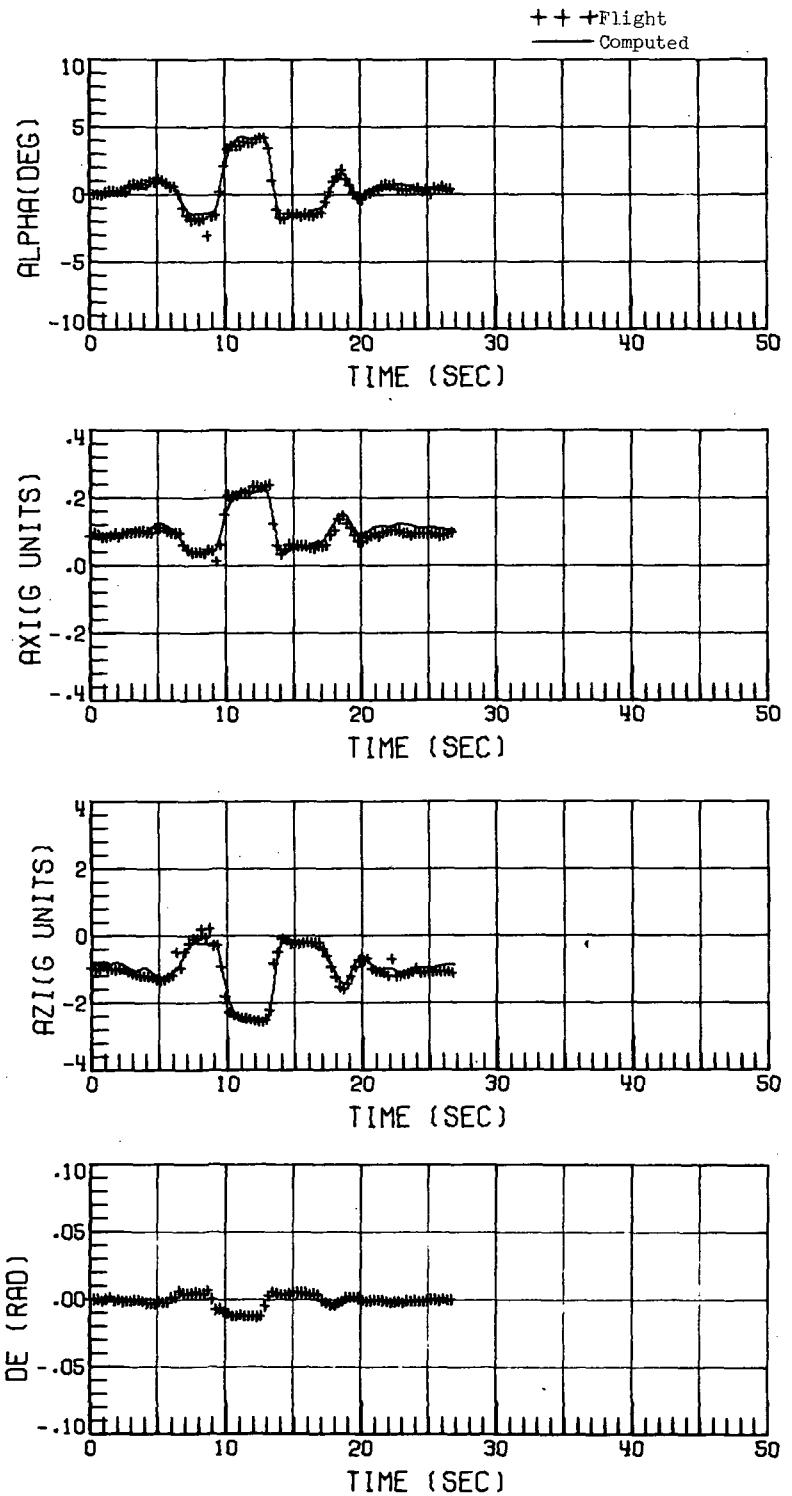

(b) $\theta_j = 15^o$. Concluded.

Figure 3.- Continued.

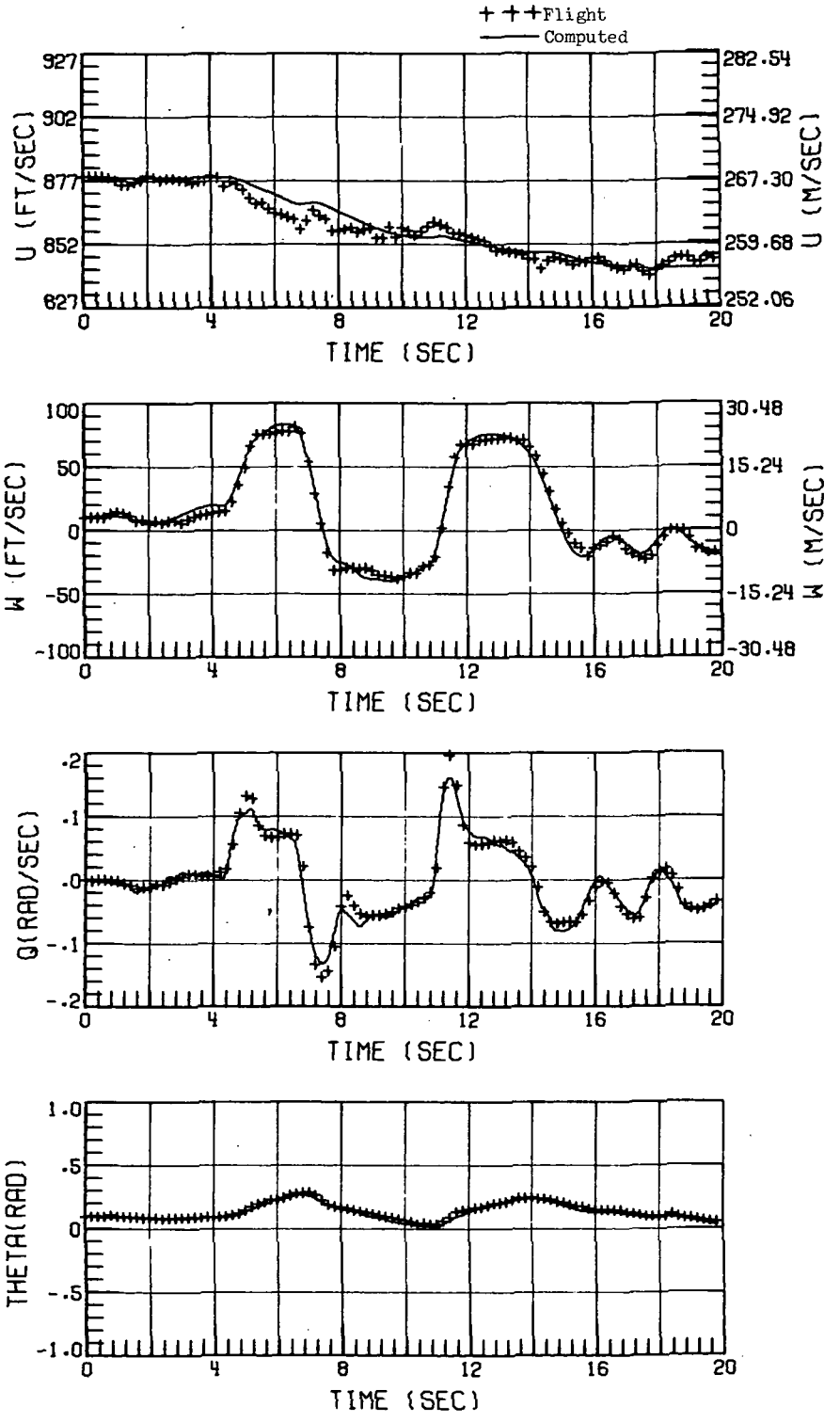

(c) $\theta_j = 30^o$.

Figure 3.- Continued.

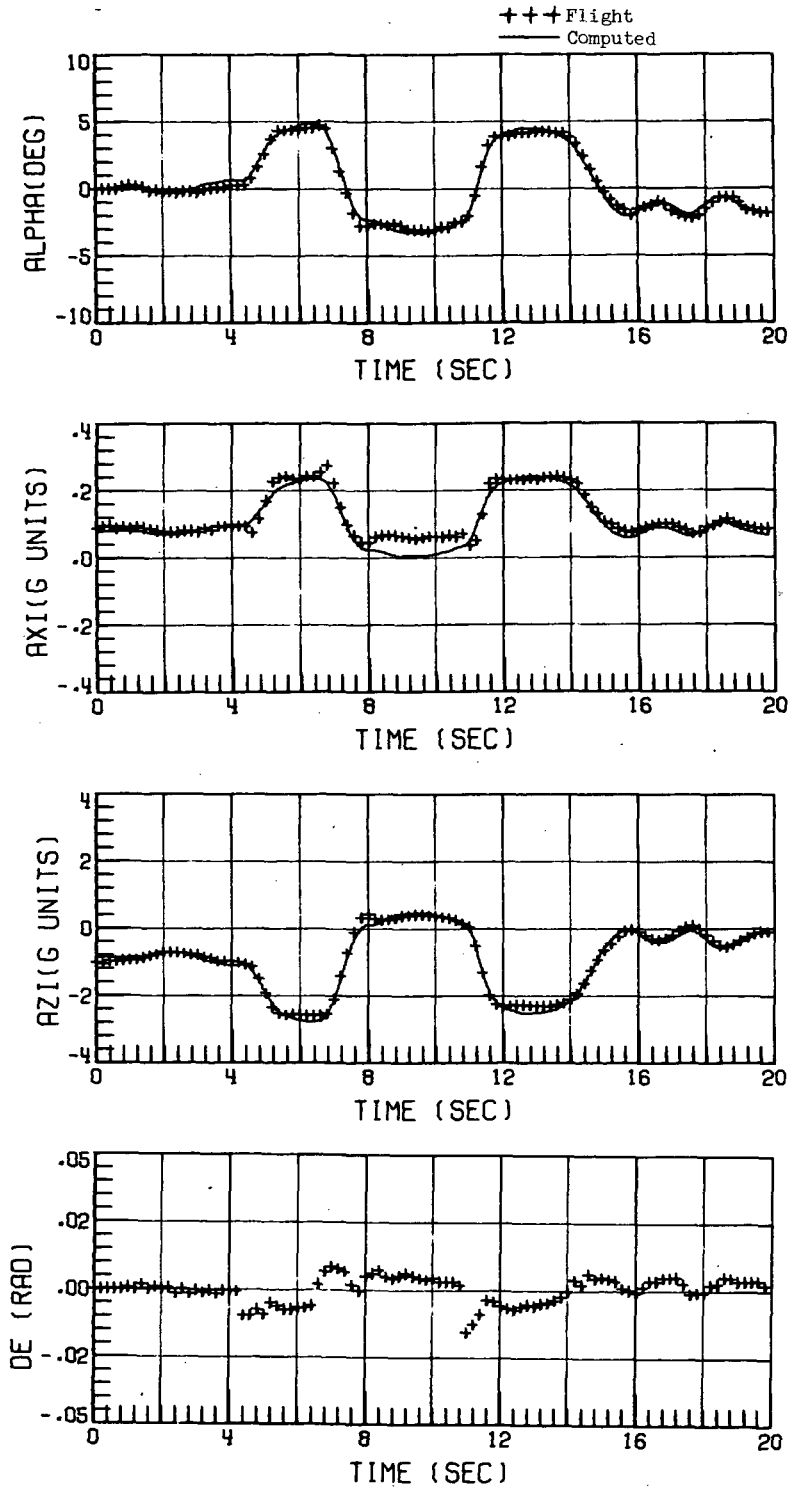

(c) $\theta_j = 30^o$. Concluded.

Figure 3.- Concluded.

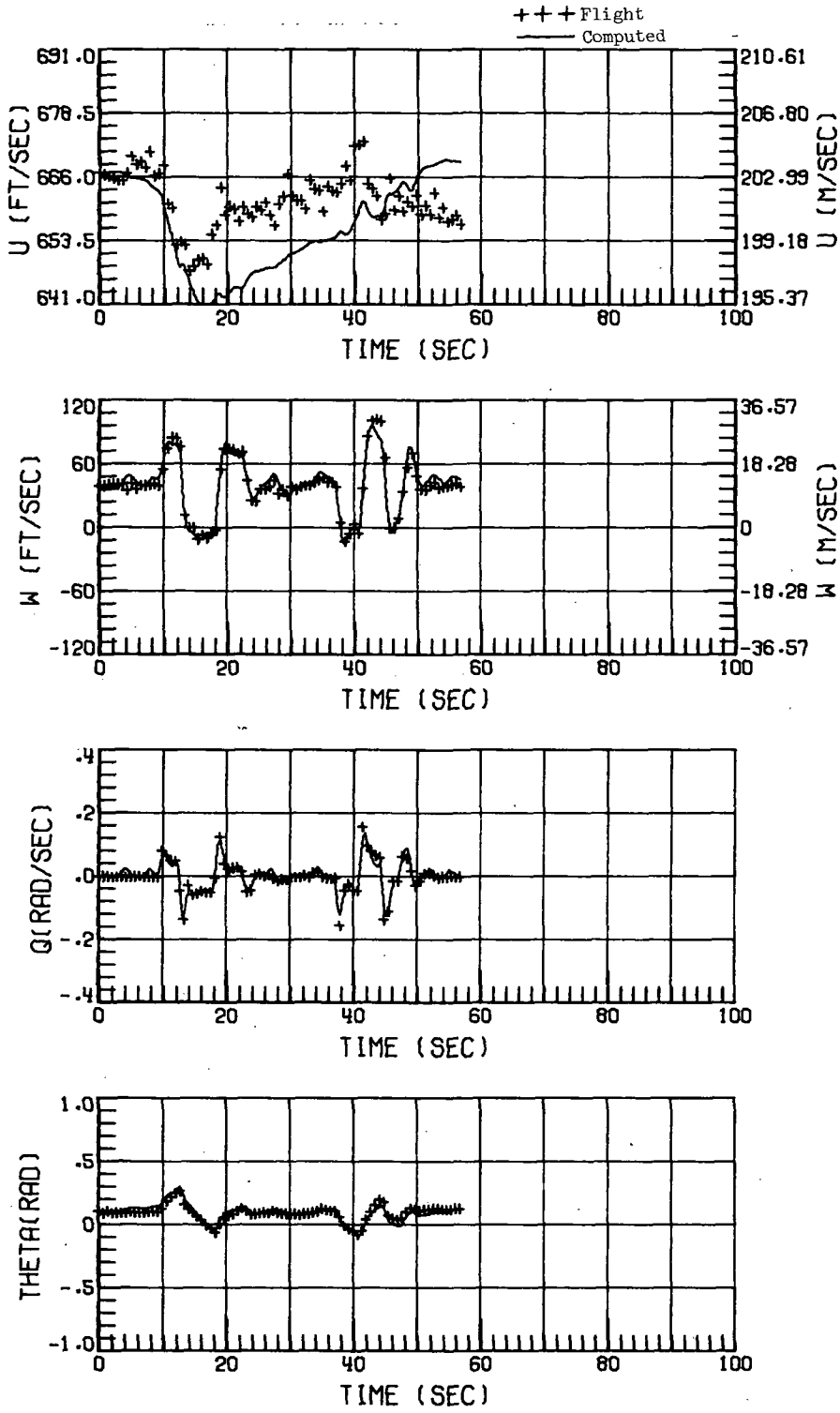

(a) $\theta_j = 0^o$.

Figure 4.- Comparison of flight data with time histories computed by using the aerodynamic parameters of table V for an elevator input. Mach number, 0.62.

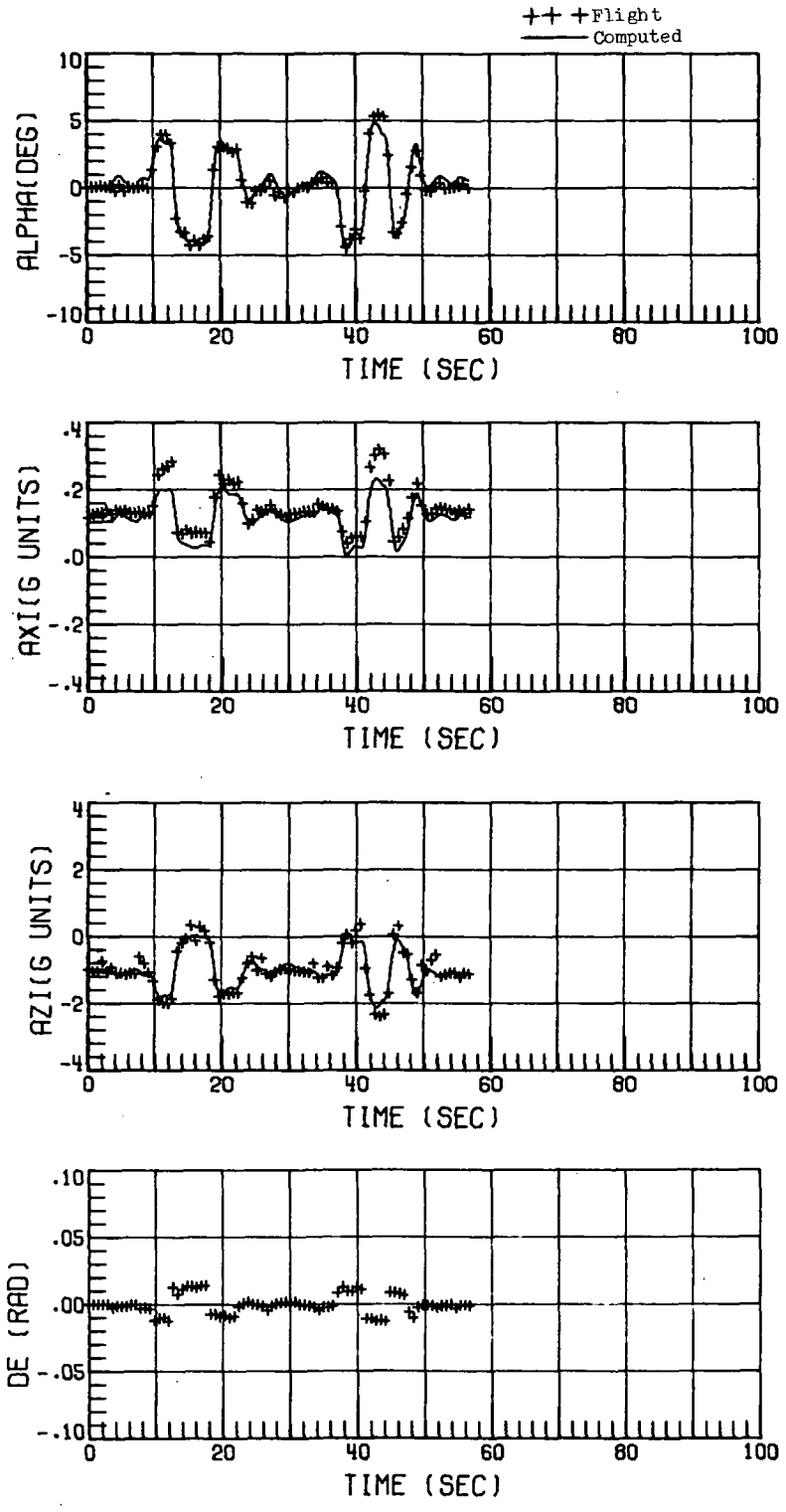

(a) $\theta_j = 0^o$. Concluded.

Figure 4.- Continued.

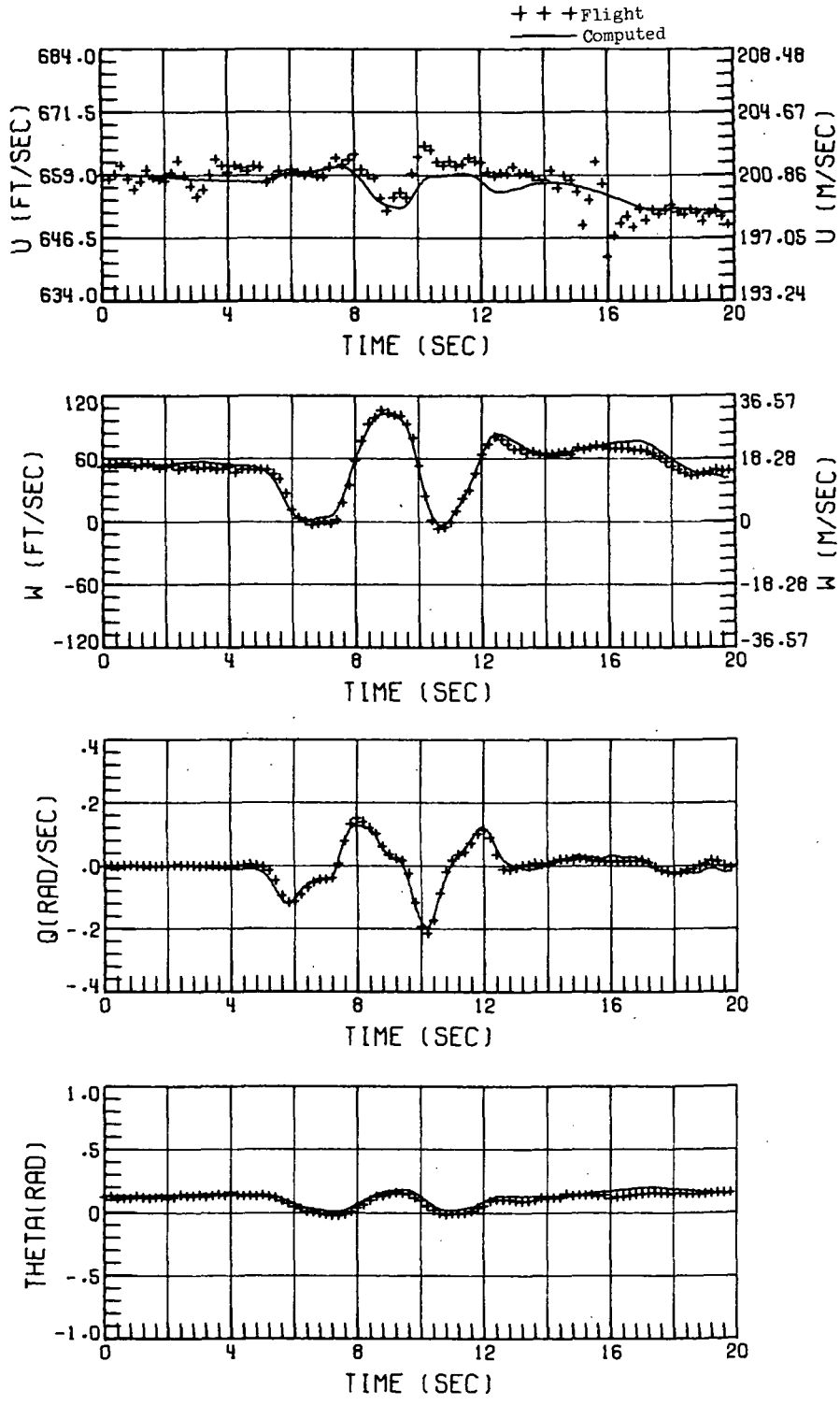

(b) $\theta_j = 15^o$.

Figure 4.- Continued.

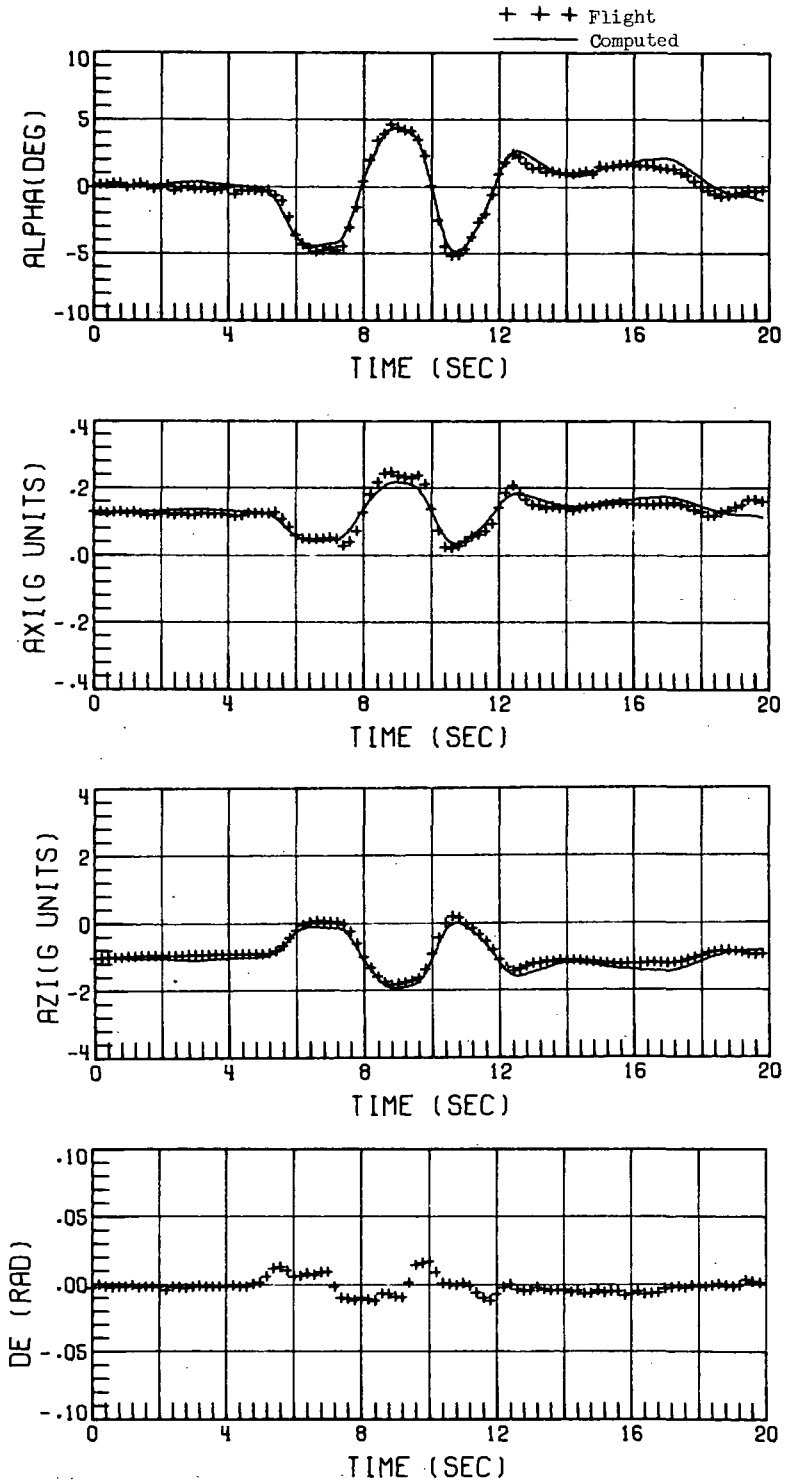

(b) $\theta_j = 15^o$. Concluded.

Figure 4.- Continued.

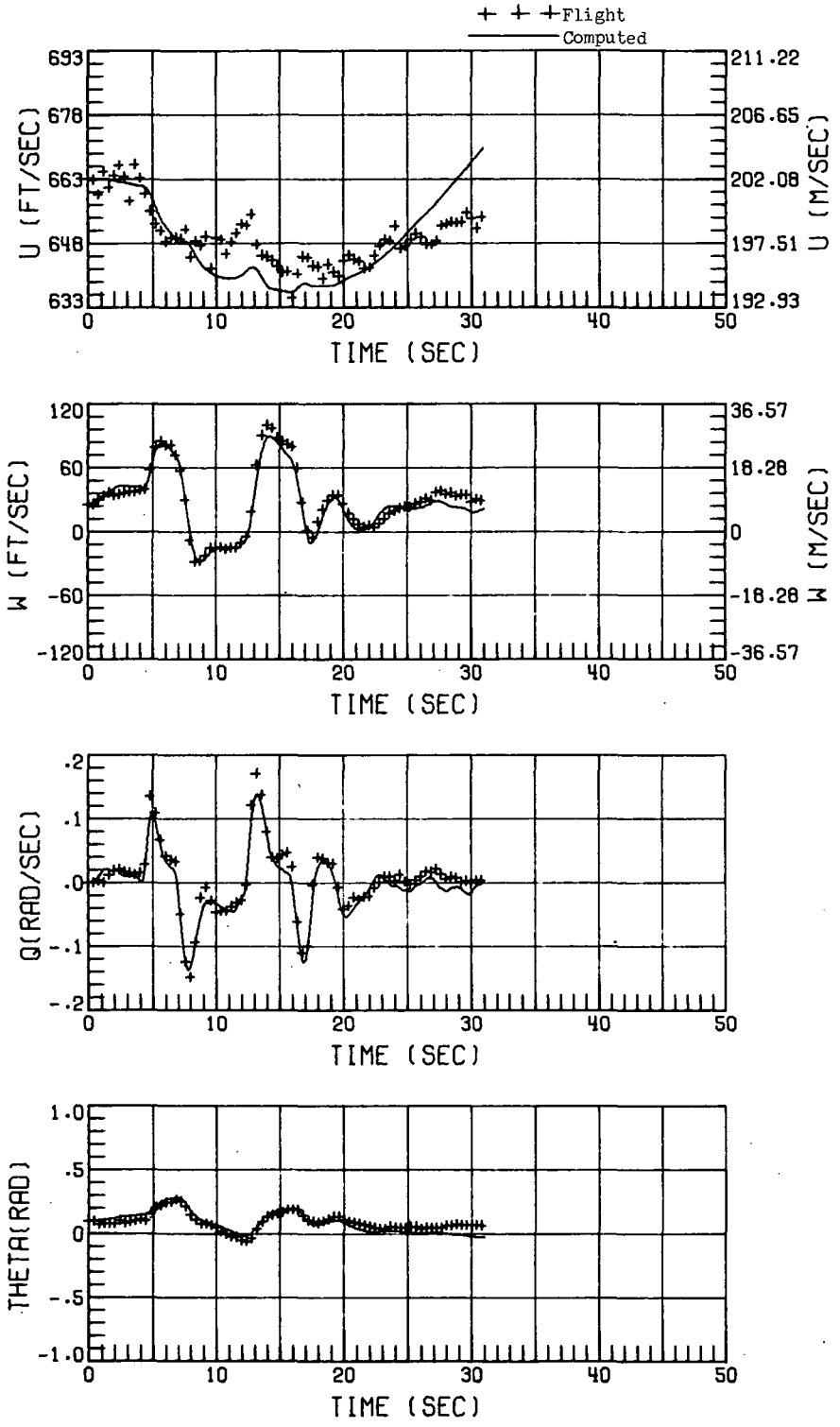

(c) $\theta_j = 30^o$.

Figure 4.- Continued.

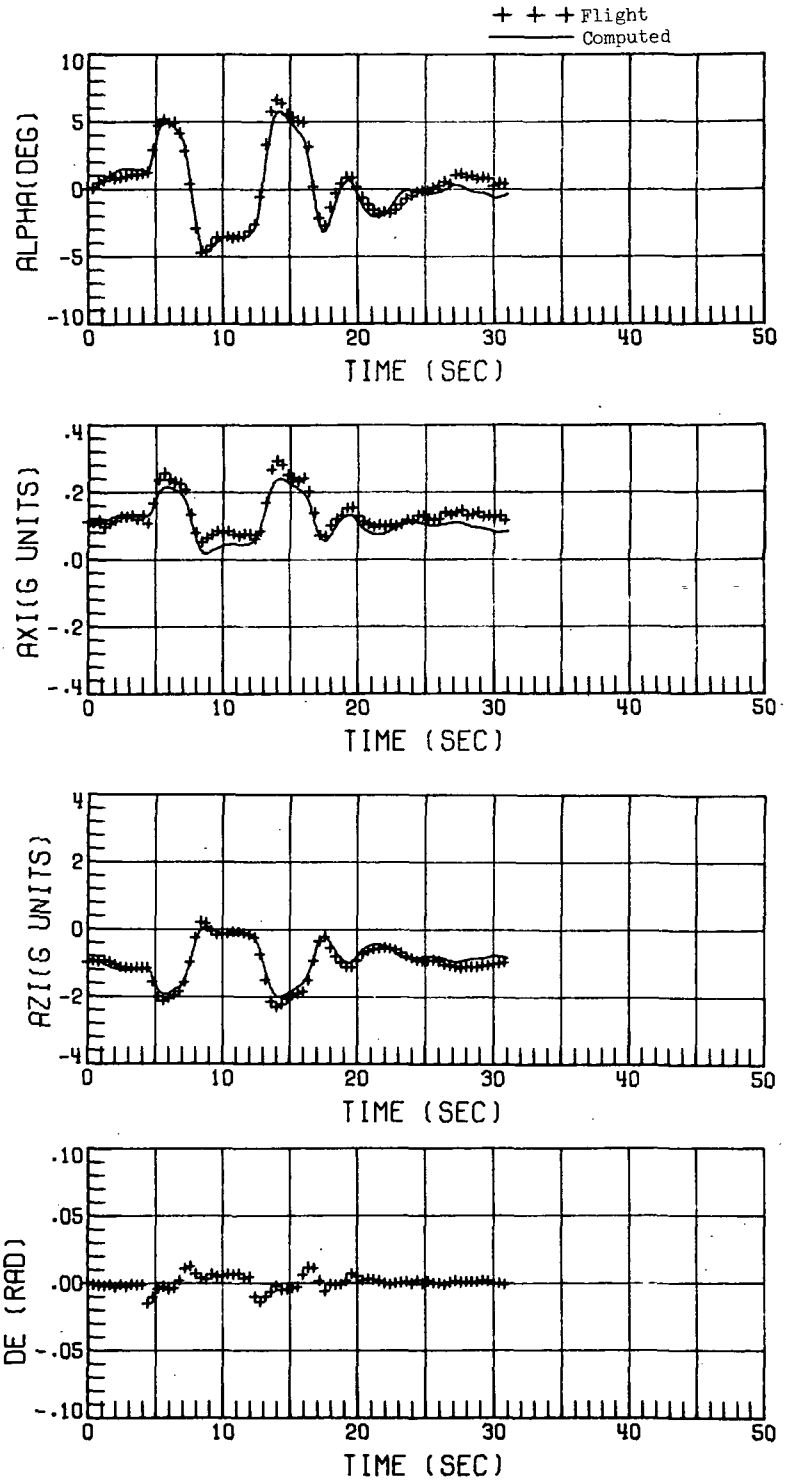

(c) $\theta_j = 30^o$. Concluded.

Figure 4.- Concluded.

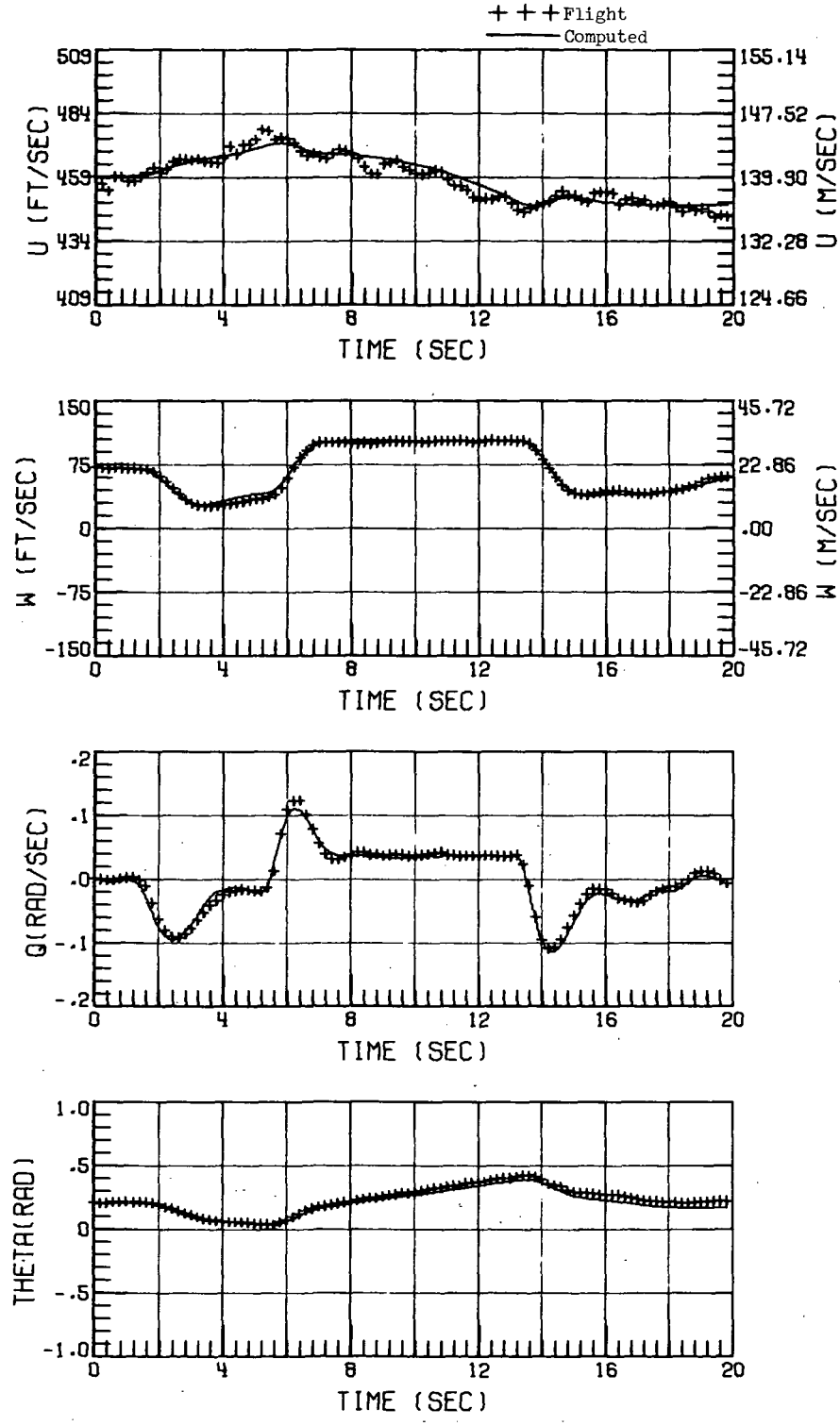

(a) $\theta_j = 0^o$.

Figure 5.- Comparison of flight data with time histories computed by using the aerodynamic parameters of table V for an elevator input. Mach number, 0.43.

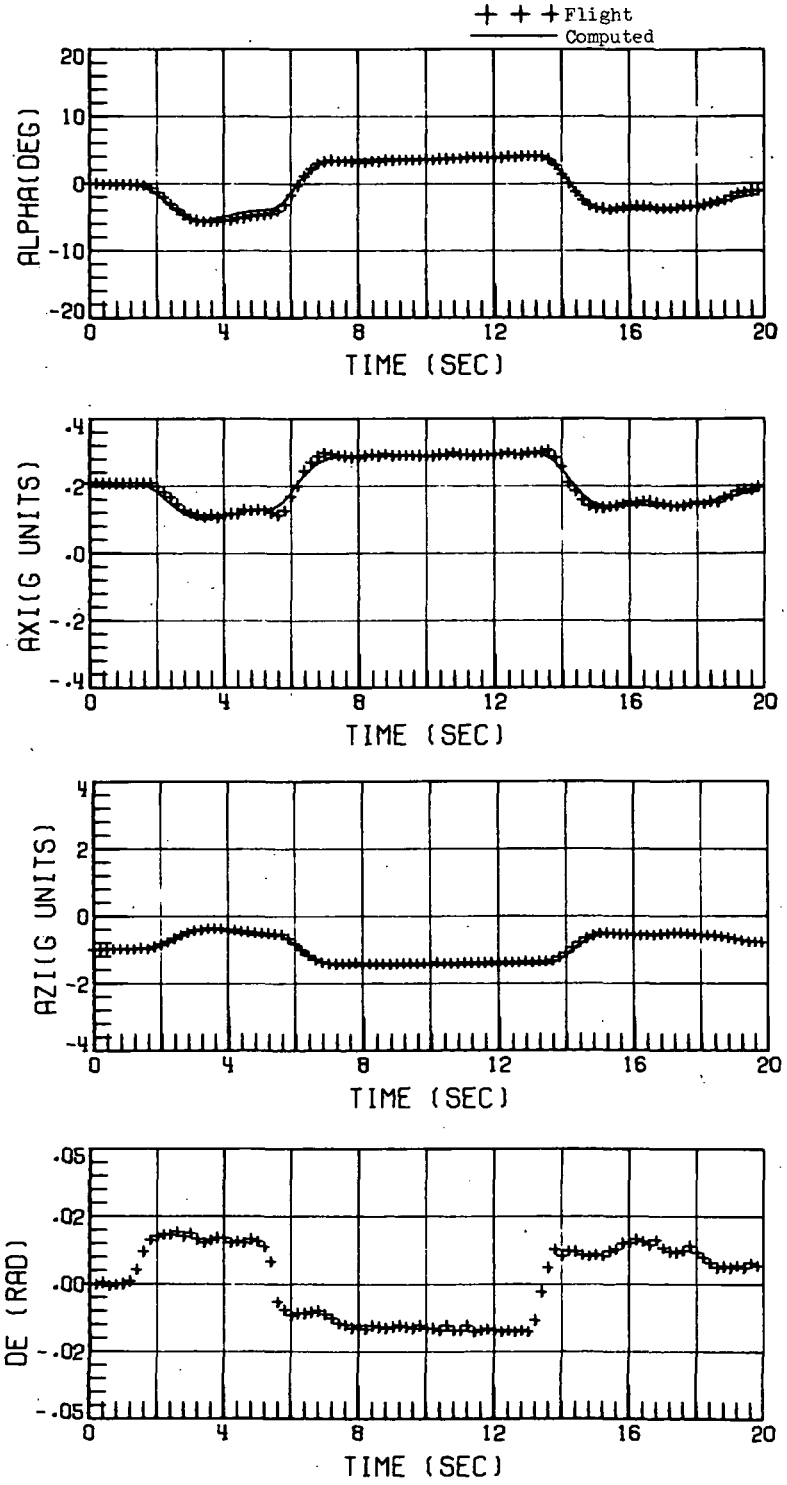

(a) $\theta_j = 0^o$. Concluded.

Figure 5.- Continued.

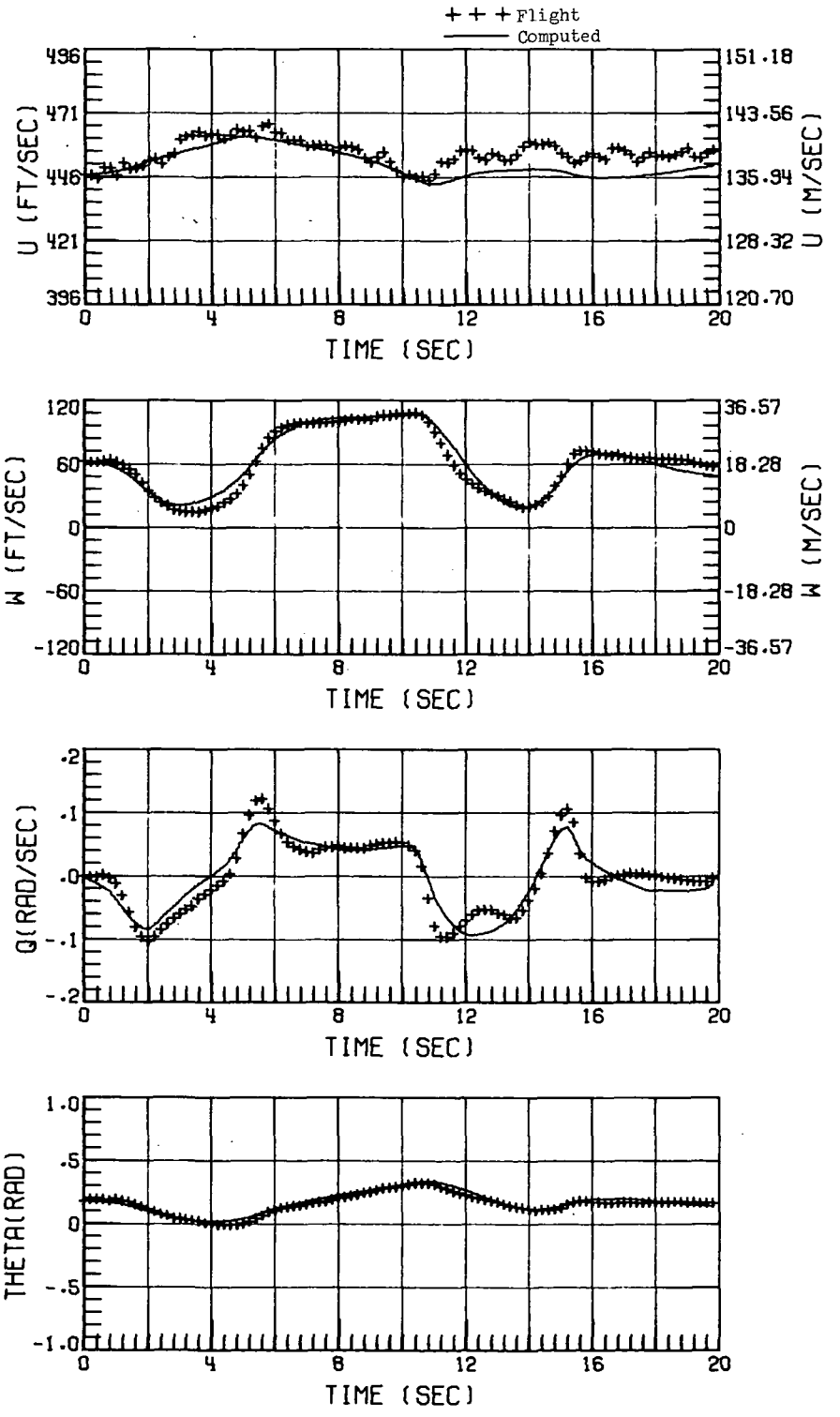

(b) $\theta_j = 30^o$.

Figure 5.- Continued.

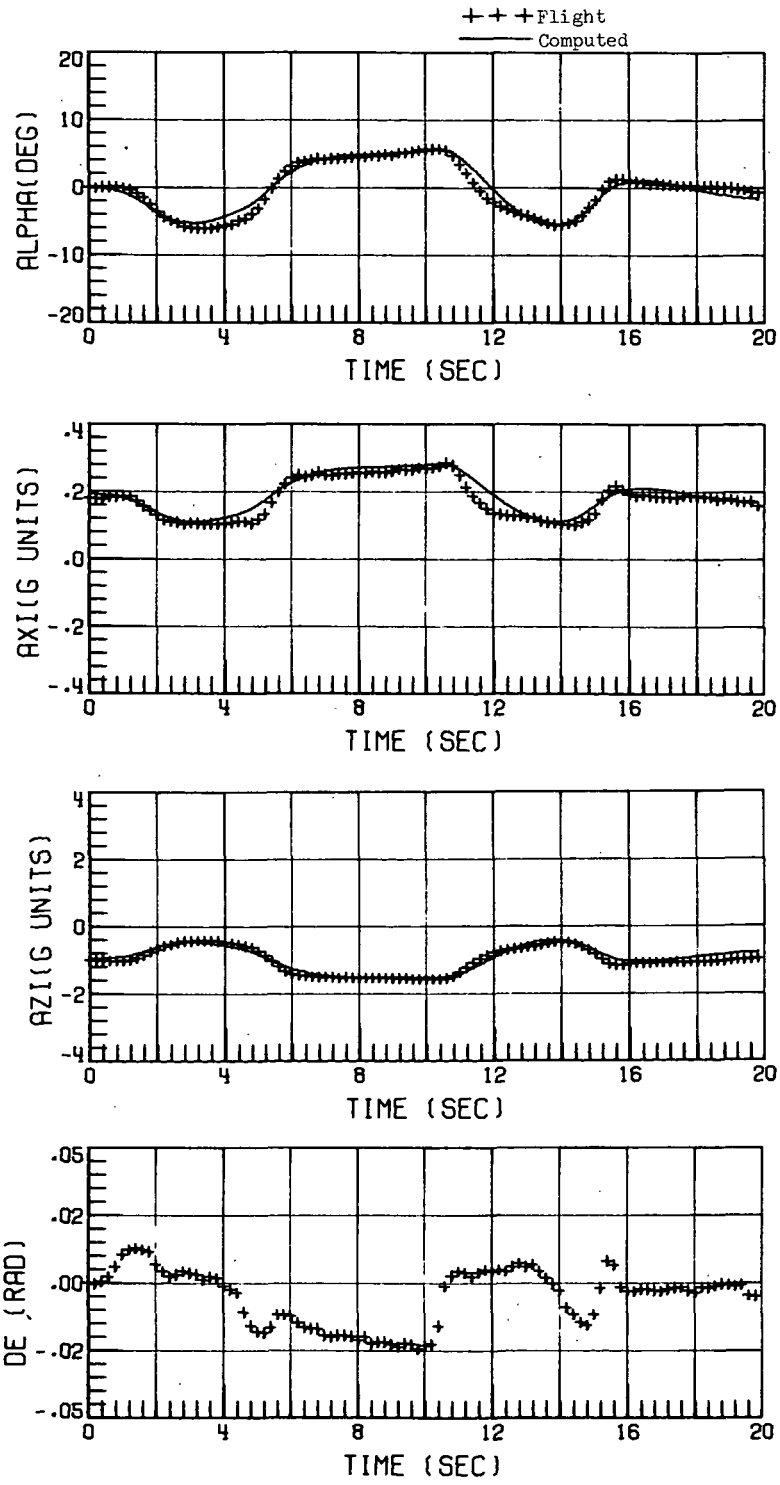

(b) $\theta_j = 30^o$. Concluded.

Figure 5.- Concluded.

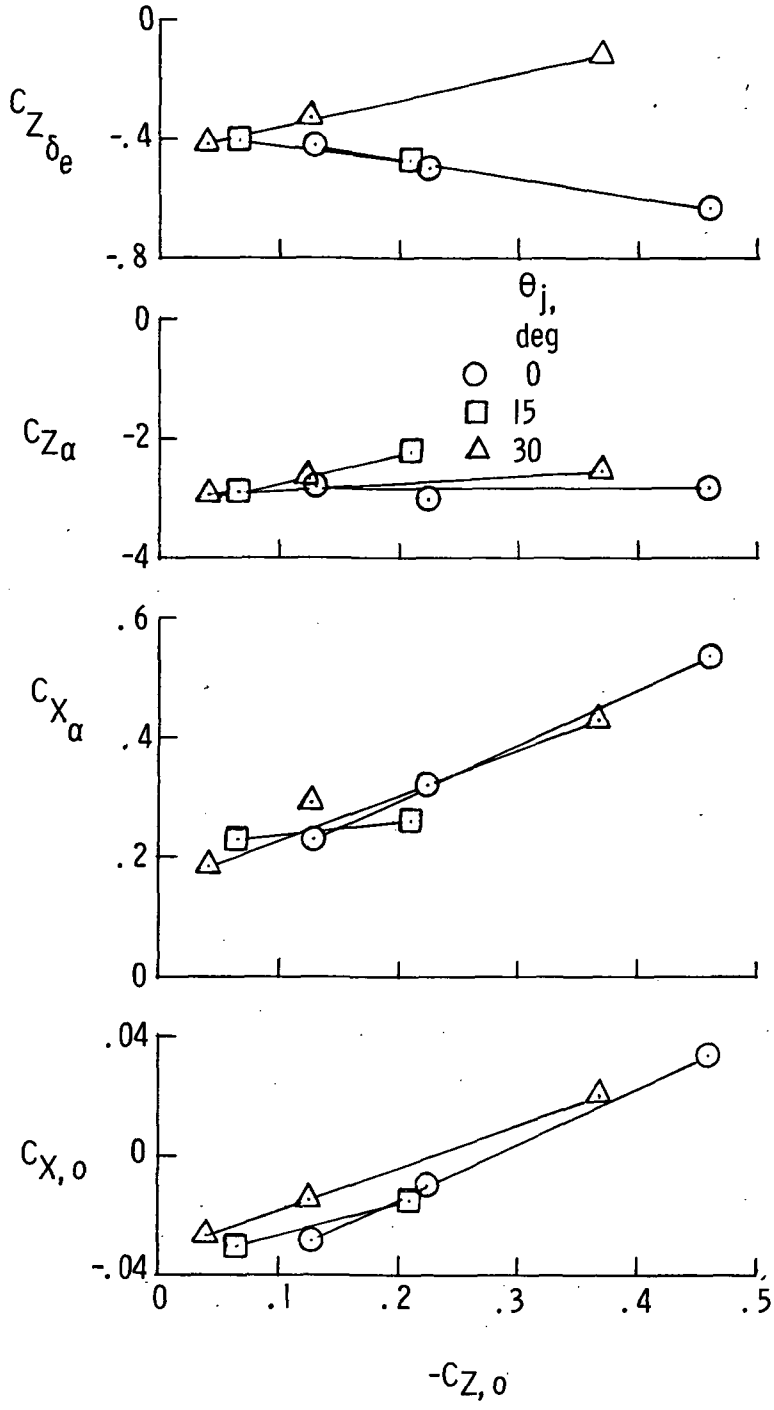

Figure 6.- Various longitudinal aerodynamic derivatives plotted against trim lift coefficient.

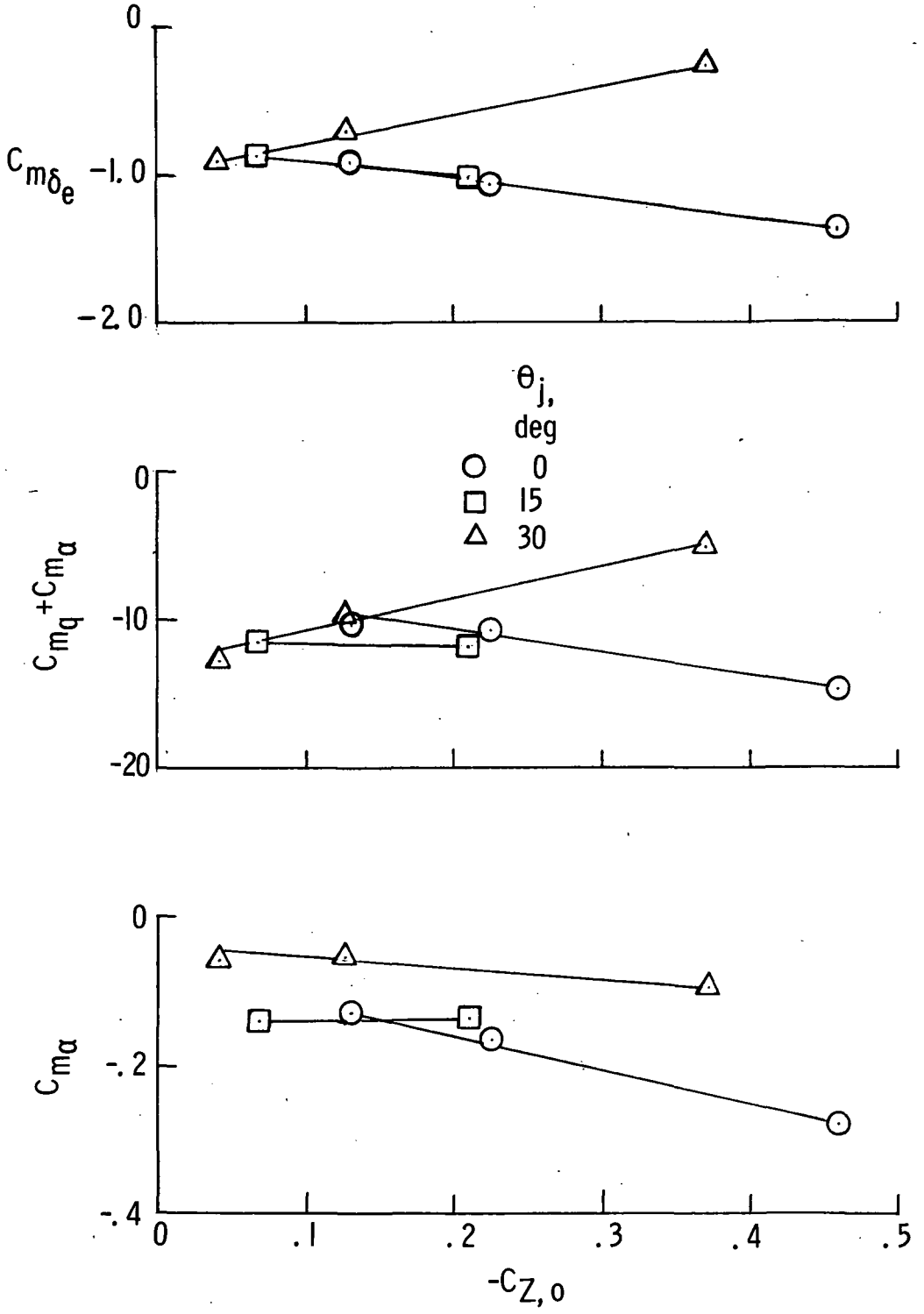

Figure 6.- Concluded.

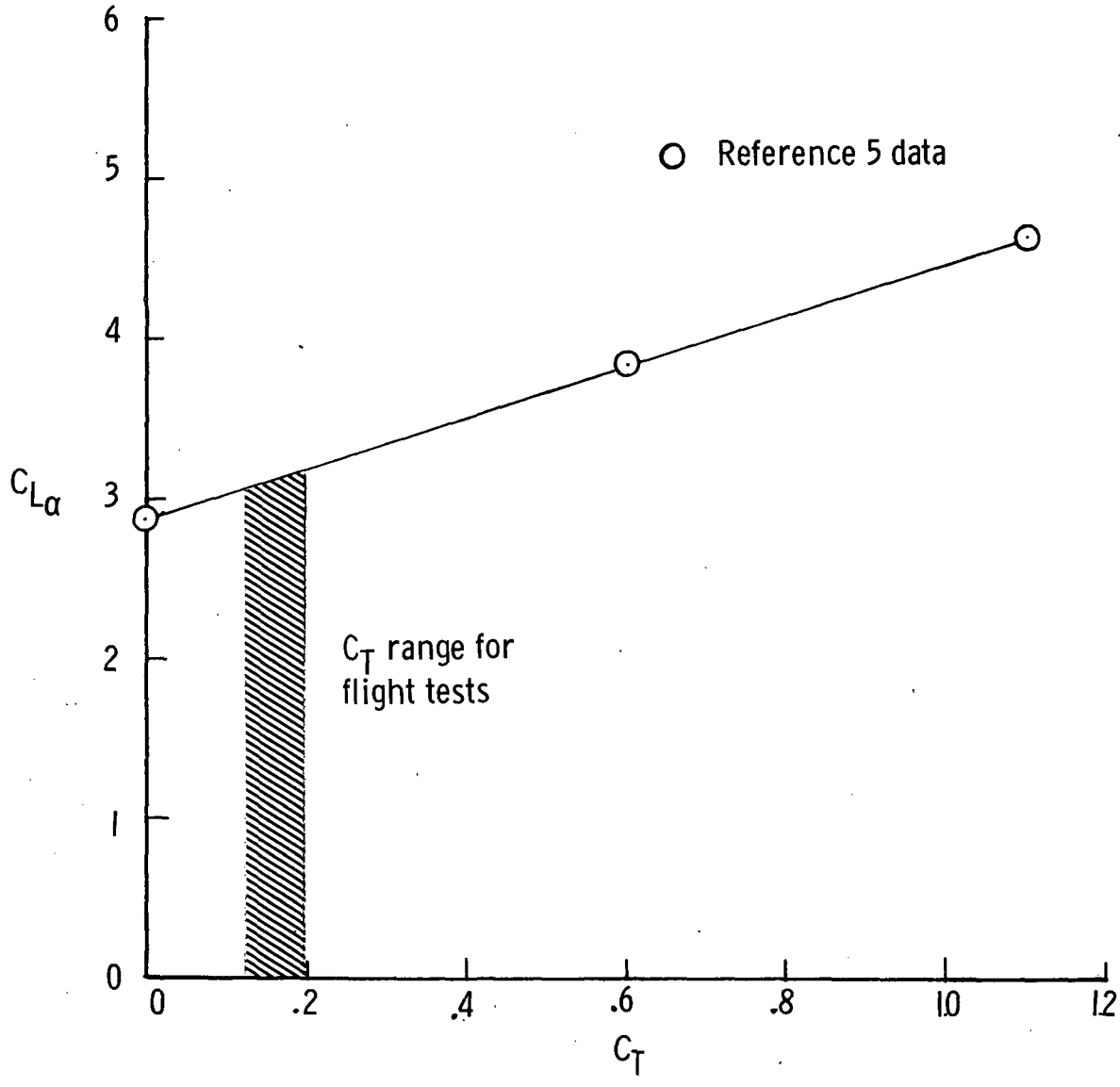

Figure 7.- Variation of C_{L_α} with C_T (from ref. 5).

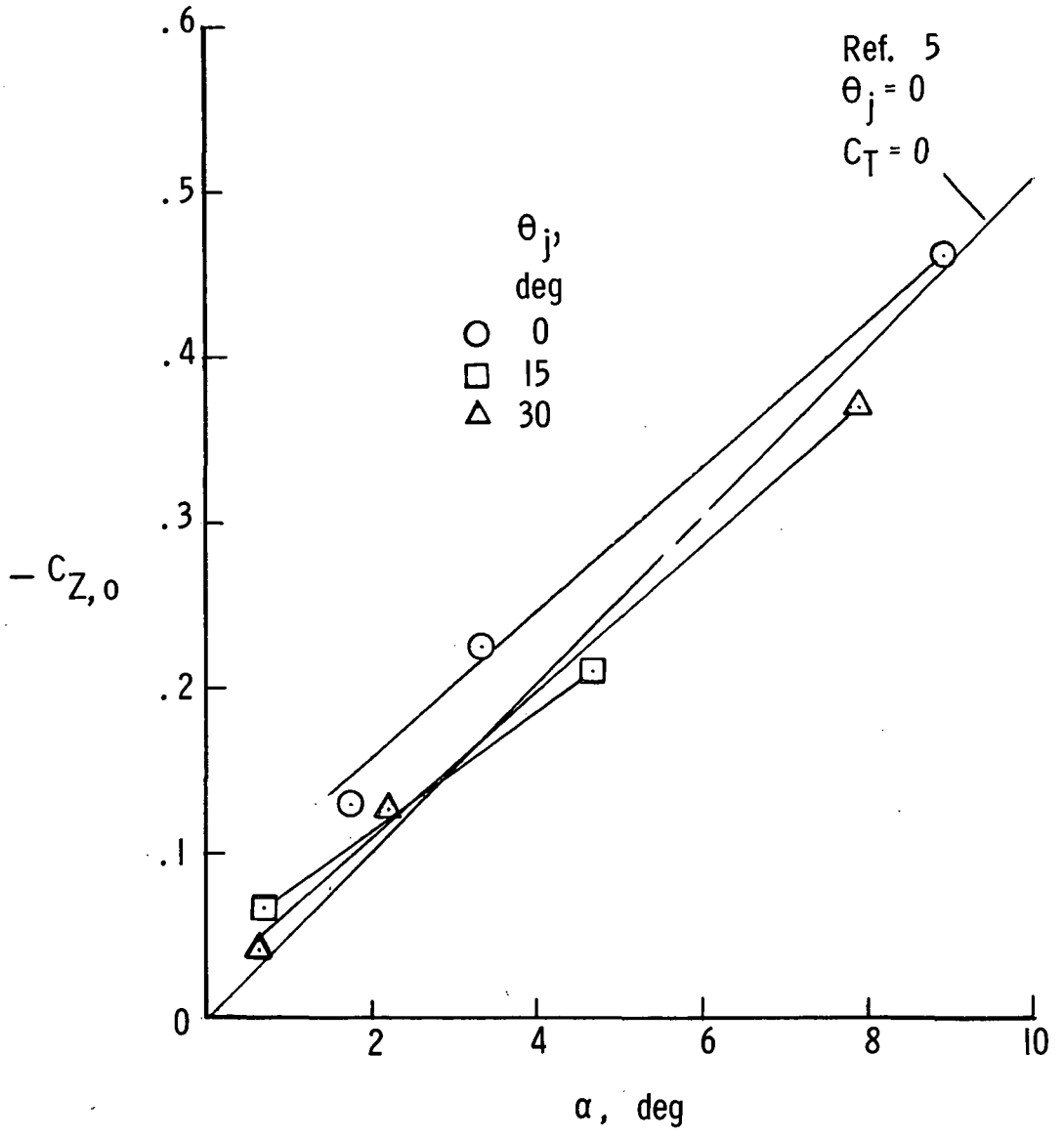

Figure 8.- Variation of $-C_{Z,o}$ with angle of attack for several θ_j settings.

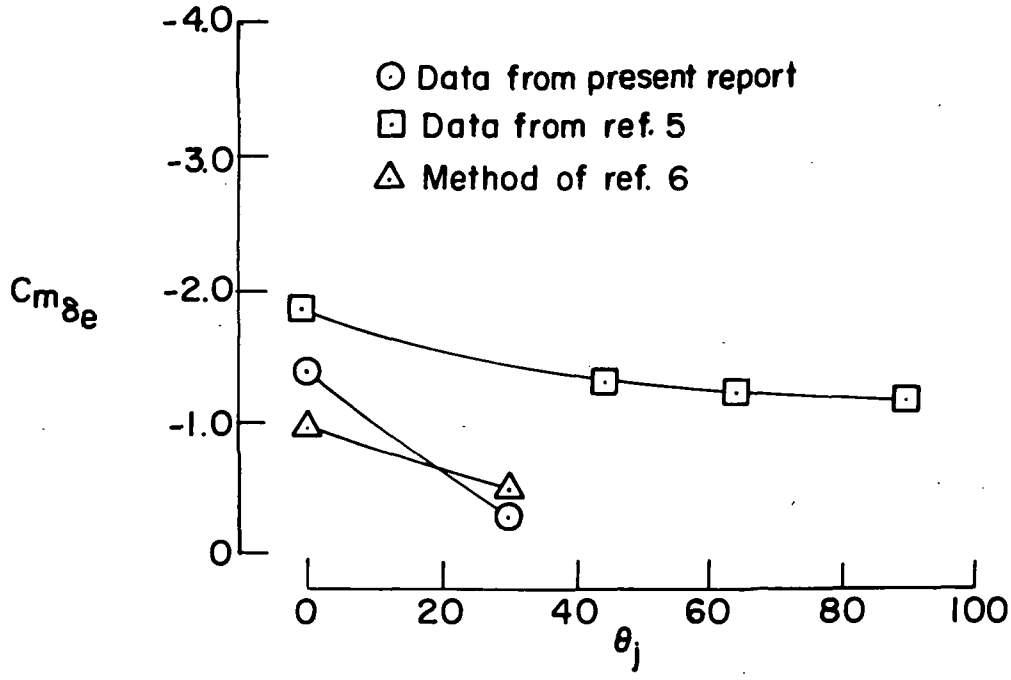

Figure 9.- Variation of $C_{m_{\delta_e}}$ with thrust deflection angle θ_j for a Mach number of 0.43.

NASA-Langley, 1973 —— 2 L-8703